Hydraulic suppression of basal glacier melt in sill fjords

Johan Nilsson[1,2], Eef van Dongen[1,2], Martin Jakobsson[3,2], Matt O'Regan[3,2], and Christian Stranne[3,2]

[1]Department of Meteorology, Stockholm University, 10691 Stockholm, Sweden
[2]Bolin Center for Climate Research, Stockholm University, 10691 Stockholm, Sweden
[3]Department of Geological Sciences, Stockholm University, 10691 Stockholm, Sweden

Correspondence: J. Nilsson (nilsson@misu.su.se)

Abstract. Using a conceptual model, we examine how hydraulically-controlled exchange flows in silled fjords affect the relationship between the basal glacier melt and the features of warm intermediate Atlantic Water (AW) outside the fjords. We show that an exchange flow can be forced to transit into the hydraulic regime if the AW interface height decreases, the AW temperature increases, or the production of glacially modified water is boosted by subglacial discharge. In the hydraulic regime, the heat transport across the sill becomes a rate limiting factor for the basal melt, which is suppressed. An interplay between processes near the ice–ocean boundary and the hydraulically-controlled exchange flow determines the melt dynamics, and the sensitivity of the basal melt to changes of the AW temperature is reduced. The model results are discussed in relation to observations from Petermann, Ryder, and 79°N glaciers in North Greenland.

1 Introduction

In response to global warming, the Greenland Ice Sheet (GIS) has lost mass over the past decades and its marine outlet glaciers are retreating (Mouginot et al., 2019; Straneo and Heimbach, 2013; Wood et al., 2021). GIS holds an ice volume equivalent to 7.4 m of sea level (Morlighem et al., 2017), and it may contribute with up to 0.3 m sea-level rise by the end of this century (Aschwanden et al., 2019). Over half of the recent mass loss from GIS is by increased discharge of ice into the ocean from marine outlet glaciers (Mouginot et al., 2019), where calving and oceanic melt of marine ice have increased. Loss of marine ice can cause a positive feedback: resistive stresses in grounded or floating marine glaciers buttress ice inland, and ice-stream flow speed and ice export across the grounding line increase when marine glaciers retreat (Schoof, 2007; Gudmundsson, 2013; Nick et al., 2013; Khazendar et al., 2019). This accelerated ice loss contributes directly to sea-level increase.

The basal melt on marine glaciers is primarily controlled by the excess ocean temperature over the (pressure dependent) freezing temperature at the grounding line (Holland and Jenkins, 1999), the point where the ice begins to float. The melt depends also on factors such as basal slope, subglacial freshwater input, tidal currents, and water column stratification (Jenkins, 2011; Truffer and Motyka, 2016). The ice melt mixes with ocean water, which creates a buoyant melt water plume that raise along the base of the ice tongue (Lewis and Perkin, 1986). Turbulence in the melt water plume transport heat to the ice–ocean boundary and sustains melt in the rising plume. Marine glaciers in Greenland terminate in fjords, and basal melt is chiefly driven by heat supplied in subsurface Atlantic Water (AW) that enters the fjords (Straneo et al., 2012). In Greenland, basal melt is sensitive to the AW temperature (Straneo and Heimbach, 2013), and increases in AW temperature have been the major driver

of the retreat of outlet glaciers in deep Greenlandic fjords since the mid 1990s (Wood et al., 2021). However, local features, such as fjord geometry and wind conditions, affect the sensitivity of the basal melt to changes of the AW temperature in the open ocean (Straneo and Cenedese, 2015; Khazendar et al., 2019; Wood et al., 2021).

The present study is motivated by recent observations of hydraulically-controlled exchange flows at sills in the Greenlandic fjords that host the ice tongues of Ryder and 79°N glaciers (Jakobsson et al., 2020; Schaffer et al., 2020). The hydraulic control sets an upper limit on the exchange flow that depends on sill geometry and upstream stratification (Pratt and Whitehead, 2007). Accordingly, hydraulic control limits the heat transport that sustains the basal melt, and can stabilise marine glaciers. Moreover, Jakobsson et al. (2020) and Schaffer et al. (2020) show that as inflowing AW passes over the sills and descends on the landward slopes, it mixes with overlaying cold glacially-modified water. As a result, the waters reaching these glaciers' grounding lines are colder than the AW outside the fjords. This reduces the basal melt compared to the case when unmodified AW reaches the glacier. Thus, hydraulic control can reduce basal melt by limiting the exchange flow as well as by decreasing the water temperature at the grounding line of the glacier.

The feature that hydraulic control (and/or fjord geometry) can limit the heat transport suggests that there are two different regimes of ice-tongue basal melt in fjords. First, one where the basal melt is controlled locally by turbulent processes near the ice–ocean boundary, which determines the heat flux from the fjord water to the ice (Fig. 1a). In this scenario, the fjord-scale circulation adjusts to deliver the heat required for the basal melt, and AW reaches the grounding line of the ice tongue. Second, in sill fjords hydraulic control may be established, which constrains the exchange circulation in the fjord and its associated heat transport (Fig. 1b). In this case, the basal melt is not solely controlled by local processes near the ice–ocean boundary, as the fjord-scale heat transport towards the glacier enters as a rate limiting factor. In the relatively narrow Greenlandic fjords, sill geometry is likely to be a major factor constraining ocean heat transport towards marine glaciers. For large Antarctic ice shelves, effects due Earth's rotation are important and the oceanic heat flux available for basal melt may be controlled by mesoscale ocean eddies or large-scale flows constrained by conservation of potential vorticity (Little et al., 2008; Hattermann et al., 2014; Zhao et al., 2019).

The observations from Ryder and 79°N glaciers (Jakobsson et al., 2020; Schaffer et al., 2020) raise the question of how strongly hydraulic control limits basal melt, and how it affects the dependence of basal melt to the temperature and height of the AW layer outside the fjords. Here, we examine this question using a conceptual two-layer fjord model that includes ocean–glacier interactions. The model results are discussed in relation to observations from the Greenlandic ice tongues of Petermann, Ryder and 79°N glaciers. However, the model can be also applied to fjords with tidewater glaciers. Before the model is presented, we give a brief overview of the oceanographic conditions at Petermann and Ryder glaciers.

1.1 Ryder and Petermann glaciers

Figures 2 and 3 shows bathymetric and temperature conditions in Sherard Osborn and Petermann fjords, where Ryder and Petermann glaciers drain. In Petermann Fjord, which has a relatively deep and wide sill, AW with similar features are encountered inside as well as outside the fjord, and there are no indications of hydraulic control at the sill (Johnson et al., 2011; Jakobsson et al., 2020).
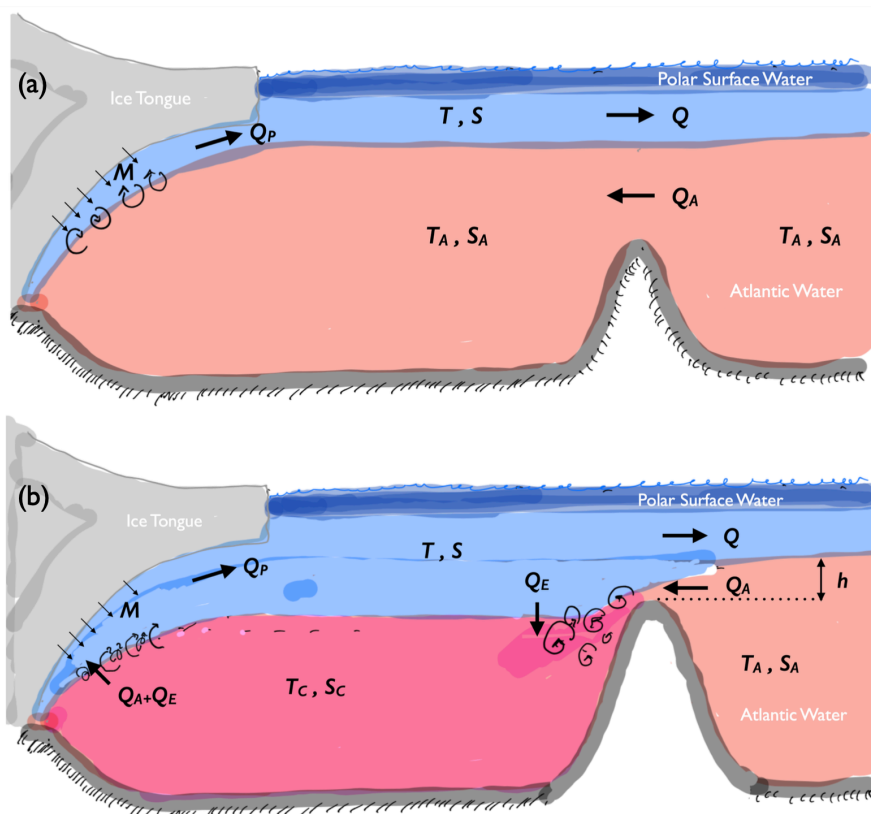
Figure 1. Oceanographic characteristics in Greenlandic fjords with ice tongues (or tidewater glaciers), showing the two-layer model described in section 2. Warm Atlantic Water (AW, with temperature and salinity T_A and S_A) is encountered at depth outside the fjord. Above the AW, there is a layer of colder outflowing glacially-modified water (T and S), which is capped by low salinity Polar Surface Water. Two flow regimes are shown: (a) a melt-controlled regime, where the exchange flow is unconstrained and AW reaches the grounding line; (b) a hydraulically-controlled regime, where outflowing water mixes with inflowing AW, thereby reducing the temperature and salinity reaching the grounding line (T_C, S_C). Model variables, listed in table 1, include AW inflow (Q_A), the outflow of glacial water (Q), entrainment into the inflowing AW (Q_E), plume flow at ice base (Q_P), and basal melt (M). The AW height above the sill (h) and the layer density difference determine the exchange flow in the hydraulically-controlled regime.
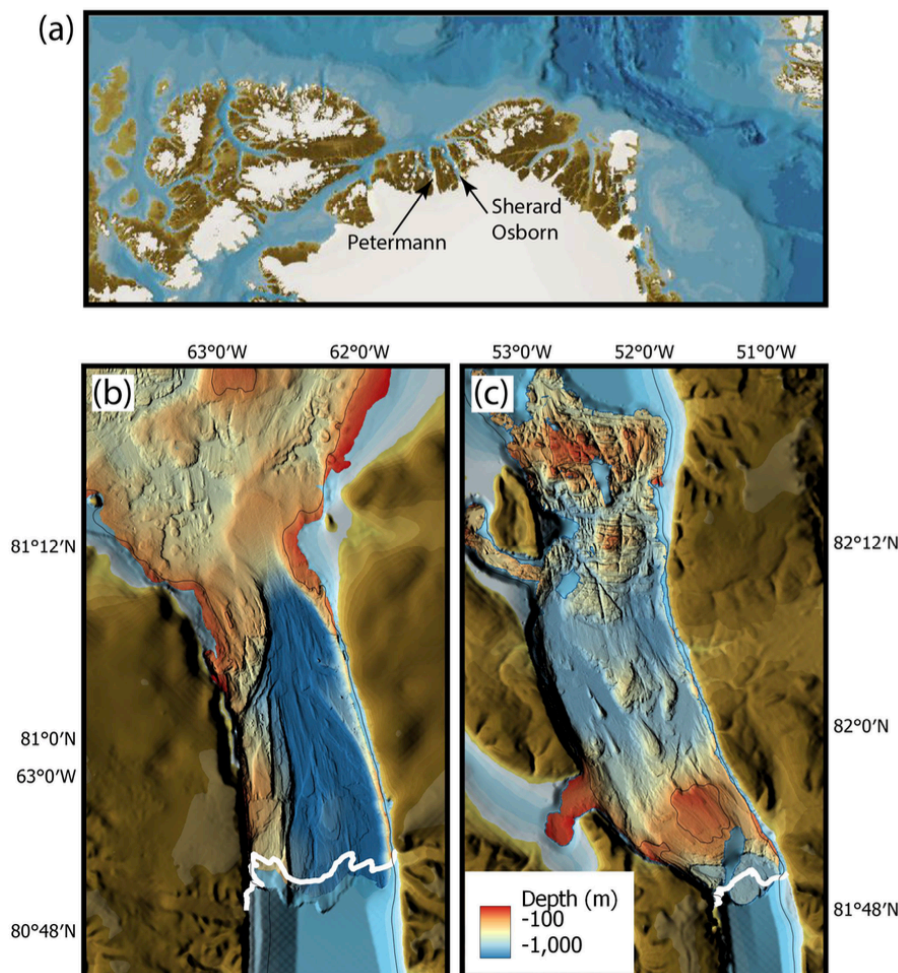
Figure 2. (a) Location of Petermann and Sherard Osborn fjords in North Greenland, where Petermann and Ryder glaciers drain. Bathymetry in Petermann (b) and in Sherard Osborn (c) fjords (Jakobsson et al., 2020); the white lines indicate the frontal positions of the ice tongues in 2019. Ryder's ice tongue is about 30 km long, and about 800 (150) m thick at the grounding line (front). Sherard Osborne Fjord has two sill: an inner sill about 10 km seaward of the ice tongue front, and an outer sill about 50 km seaward of the ice tongue front. The deepest passage over the inner sill is a one kilometer wide, 400 m deep channel on the eastern side.

60   Sherard Osborn Fjord has a more constrictive fjord topography, with an outer and an inner sill. The temperature in the AW depth range decreases across the sills, with the coldest temperature in the fjord basin landward of the inner sill that is largely capped by the ice tongue. The largest temperature drop occurs over the inner sill. Here, a strong near-bottom inflow was observed, occurring in a $\sim$400 m deep and $\sim$1 km wide channel on the eastern sill, demonstrating that the inflow is hydraulically controlled (see Fig. 4 in Jakobsson et al., 2020). Accordingly, the inner sill provides the main geometrical constraint on the

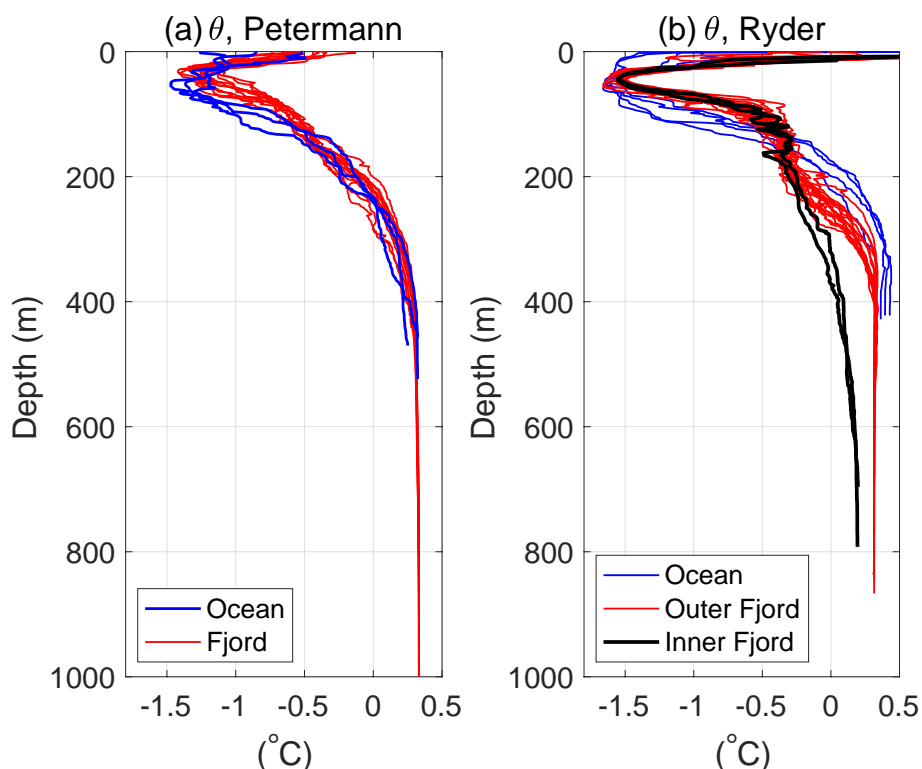65   exchange flow and heat transport to the glacier.

4

Figure 3. Potential temperature profiles from Petermann Fjord (a) and Sherard Osborne Fjord (b). The observations where taken in August 2019 during the Ryder Expedition with the icebreaker *Oden*, see Jakobsson et al. (2020) and Stranne et al. (2021) for further information on the conditions in the fjords. Sherard Osborne Fjord has two sill: progressing into the fjord, the AW temperature drops as the sills are crossed. The present focus is on the inner sill separating the inner and outer fjord basins. Petermann has a single wider and deeper sill, and here AW reaches the glacier's grounding line in the fjord.

During the last six decades the ice tongues of Petermann and Ryder have evolved differently: the former retreating significantly (∼300 m per year) and the latter advancing modestly (∼40 m per year) (Hill et al., 2018); and in 2010 and 2012 Petermann lost ∼35 km of its tongue in major calving events (Johannessen et al., 2013). The two glaciers are relatively closely located and are expected to experience similar atmospheric condition and to have AW of similar temperatures outside the fjords. Jakobsson et al. (2020) proposed that the differences in fjord bathymetry is the reason for different behaviour of the two glaciers: Ryder Glacier has a more restrictive sill geometry, partly protecting the ice tongue from inflow of warmer subsurface AW (Fig. 2).

In summary, these results suggest tentatively that the basal melt on Petermann is chiefly rate limited by processes near the ice–ocean boundary, whereas the basal melt on Ryder is partly rate limited by large-scale heat transport towards the glacier. In addition to differences in sill geometry, differences in summer sea-ice conditions influence the efficiency in transporting AW into the two fjords. Perennial land-fast sea ice outside Sherard Osborne Fjord curtail wind-driven water exchange between the

fjord and the open ocean; whereas ice-free condition in and around Petermann Fjord allows for a more vigorous wind-driven water exchange during summer (Shroyer et al., 2017; Jackson et al., 2018; Stranne et al., 2021).

2 A two-layer model

We consider a two layer model of glacier–ocean interaction in a fjord, with AW (T_A,S_A) and glacially modified water (T,S) (see Straneo and Cenedese, 2015; Jackson and Straneo, 2016, for a background). Figure 1 shows the model geometry for two different circulation regimes that will be examined. The model represents near steady-state conditions, and we assume that the time-mean exchange flow in the fjord is primarily driven by basal melting on the ice tongue, which creates a buoyant melt water plume raising along its base. Higher up, the plume becomes neutrally buoyant and feeds the outflow of glacially modified water. A layer of polar surface water caps the two water mass represented in the model, insulating them for contact with sea ice and the atmosphere. The polar surface water is not explicitly represented in the model.

2.1 Conservation relations

In the two-layer model of the fjord, melting of the ice tongue is the only local source/sink of freshwater/heat. (Although subglacial discharge affects melt rates, we ignore it for simplicity in the freshwater budget.) This can be used to formulate conservation relations for volume, salt and heat (Jackson and Straneo, 2016; Truffer and Motyka, 2016). At the sill, conservation of volume is given by

$$Q = Q_A + M, \tag{1}$$

where Q and Q_A is the volume outflow and inflow of glacially modified and Atlantic waters respectively, and M the freshwater input due to melting. The ice consists of pure freshwater, implying that the meltwater input M does not affect the salinity budget. Hence conservation of salt is given as

$$SQ = S_A Q_A. \tag{2}$$

Combining Eqs. (1, 2) yields Knudsen's relation for salt conservation

$$\Delta S Q = S_A M, \qquad \Delta S \stackrel{\text{def}}{=} S_A - S. \tag{3}$$

The heat budget involves a balance between advective heat transport towards the glacier and basal melt. The advective heat flux is

$$H = c(T_A Q_A + T_f M - T Q), \tag{4}$$

where c is the heat capacity (per unit volume) of sea water, and the melt freshwater input M is assumed to have the salinity dependent freezing temperature T_f. Note that T_f will be taken as constant set by the grounding-line pressure and S_A. Using Eqs. (1,4), we obtain

$$H = c[\Delta T Q + (T_f - T_A)M] \qquad \Delta T \stackrel{\text{def}}{=} T_A - T. \tag{5}$$

Table 1. Definition of model variables and physical constants, see Fig. 1.

T_A, S_A, h	Atlantic Water (AW) T, S, and height
T, S	Glacially-modified water T and S
T_C, S_C	Ice cavity water T and S
$T_f = T_f(S_A, d)$	Freezing point at grounding-line depth (d)
$\Delta T = T_A - T$	Layer difference in T
$\Delta S = S_A - S$	Layer difference in S
$\mathcal{T} = T_C - T_f$	Thermal forcing
$\mathcal{T}_A = T_A - T_f$	AW thermal forcing
Q, M	Exchange flow and melt water input
Q_A, Q_P, Q_H	AW, melt-plume, and hydraulic flows
$c \approx 4 \cdot 10^6, c_i \approx 2 \cdot 10^6$	Heat capacity of water and ice (J m^{-3} K^{-1})
$L \approx 3 \cdot 10^8$	Latent heat of fusion (J m^{-3})
$T_G = L/c$	Gade temperature (≈ 80 K)

The heat flux is related to the ice melt (M) as

$$H = M[L + c_i(T_f - T_i)], \tag{6}$$

where L is the latent heat of freezing, c_i the heat capacity of ice, and T_i the ice temperature.

By combining Eqs. (5,6), we obtain

110 $$\Delta T Q = M[L/c + c_i/c(T_f - T_i) + (T_A - T_f)], \tag{7}$$

Here, $L/c \approx 80$ °C, and in North Greenlandic fjords $T_A - T_f$ is typically 3 °C. Hence, the terms involving $T_A - T_f$ can to a good approximation be neglected in Eqs. (5,7). By defining a generalised Gade temperature (Gade, 1979)

$$T_G \stackrel{\text{def}}{=} L/c + c_i/c(T_f - T_i), \tag{8}$$

Eq. (7) can be written as

115 $$\Delta T Q = T_G M, \tag{9}$$

which gives the relation between the advective heat flux and the melt. Note that unless the ice temperature is very cold $T_G \approx L/c$.

The conservation relations of the model can be summarised as follows:

1. Volume: The melt water input M is small, implying that $Q \approx Q_A$. Thus, the inflow of AW approximately equals the
120   volume outflow of glacially modified water. In what follows, we will denote the exchange flow simply by Q.

2. Salt: The salt balance is given by Eq. (3). Here, M cannot be neglected since it is multiplied by S_A, which is larger than ΔS: Relation (3) states that $M/Q = \Delta S/S_A$.

3. Heat: The heat budget is specified by Eq. (9), which in combination with Eq. (3) yields

$$\frac{\Delta S}{S_A} = \frac{\Delta T}{T_G}. \tag{10}$$

125   For melting of ice in sea water, heat and salt conservation yields a linear relationship between the salinity and temperature differences (Gade, 1979). This allows us to either use ΔT or ΔS in our analyses; we will use ΔT.

The layer density difference is calculated using a linear equation of state

$$\Delta\rho = \rho_0(\beta\Delta S - \alpha\Delta T), \tag{11}$$

where $\rho_0 = 1025$ kg m^{-3} is a constant seawater reference density, and where $\alpha = 4\cdot10^{-5}$ K^{-1} and $\beta = 8\cdot10^{-4}$ are the thermal
130   and haline expansion coefficient, respectively. Relation (10) allows the density difference to be written

$$\frac{\Delta\rho}{\rho_0} = \frac{\Delta T}{T_G}\left(\beta S_A - \alpha T_G\right). \tag{12}$$

Here, $(\alpha T_G)/(\beta S_A) \approx 0.1$ showing that the salinity dominates the density difference.

2.2 Basal melting and unconstrained exchange flow

We will use a parametrisation of the basal melt (M), which depends on the difference between the ocean water temperature
135   (T_C) and the freezing point temperature of sea water (T_f) at the grounding line (Holland et al., 2008; Jenkins, 2011; Xu et al., 2013; Favier et al., 2019). We denote the thermal forcing as

$$\mathcal{T} \stackrel{\text{def}}{=} T_C - T_f. \tag{13}$$

If AW reaches the grounding line, then $T_C = T_A$, and the thermal forcing is denoted

$$\mathcal{T}_A \stackrel{\text{def}}{=} T_A - T_f. \tag{14}$$

140   However, mixing between in- and out-flowing waters over a sill can may lower T_C relative to T_A, which implies that $\mathcal{T}$ can be lower than $\mathcal{T}_A$.

We model the area-integrated basal melt as (Xu et al., 2013)

$$M = \gamma_1 \mathcal{T}^{n_1}, \tag{15}$$

where γ_1 is a coefficient that depends on features such as the ice-tongue geometry and subglacial discharge, and n_1 an exponent.
145   We assume that also the plume volume flow Q_P is a function of the thermal forcing $\mathcal{T}$ and given by

$$Q_P = \gamma_2 \mathcal{T}^{n_2}, \tag{16}$$

8

where γ_2 is a constant and n_2 an exponent.

Several studies have used models of varying complexity to examine the relationship between thermal forcing and the area-integrated melt on Greenlandic ice tongues and Antarctic ice shelves (e.g. Jenkins, 1991, 2011; Little et al., 2009; Lazeroms et al., 2018, 2019; Holland et al., 2008; Cai et al., 2017; Favier et al., 2019). These investigations report values of n_1 in the range from 1 to 2, with a preference for n_1 values of around 1.5 (Xu et al., 2013; Cai et al., 2017) to 2.0 (Holland et al., 2008; Little et al., 2009). The reported range of n_1 is likely to reflect both different ice–ocean interaction regimes and model assumptions on the boundary conditions at the ice–ocean boundary. There are fewer studies that specifically comment on the relationship between the volume transport in the plume and the thermal forcing, but Holland et al. (2008) reported a linear dependence of Q_P on the thermal forcing, i.e. $n_2 \approx 1$.

Primarily, the heat flux to the ice and the associated melting depend on the product of the thermal forcing and the plume velocity (say u), which in turn is related to the plume buoyancy (Holland and Jenkins, 1999; Favier et al., 2019). If the plume buoyancy is proportional to $\mathcal{T}$, and the buoyancy force is balanced by a linear basal friction, then $u \propto \mathcal{T}$. This gives $n_1 = 2$ corresponding to a quadratic relation between melt and thermal forcing (Holland et al., 2008; Little et al., 2009). If the basal friction is quadratic, i.e. proportional to u^2, on the other hand, scaling analyses suggest that $u \propto \mathcal{T}^{1/2}$ (Lazeroms et al., 2018), which gives $n_1 = 1.5$. Jakobsson et al. (2020) applied the plume model of Jenkins (1991) to Ryder Ice Tongue, and their results suggest that $n_1 \approx 1.7$ and $n_2 \approx 0.7$. Notably, if $M \propto u\mathcal{T}$ and $Q_P \propto u$, then $M/Q_P \propto \mathcal{T}$. In view of Eqs. (15,16) this implies that

$$n_1 - n_2 = 1. \tag{17}$$

This special constraint on the exponents leads to some attractive simplifications of the dynamics, which will be used in the analyses.

In summary, the literature reports and range of values for n_1 and n_2. However, $n_1 = 2$ and $n_2 = 1$ appear as one reasonable choice for the exponents, and this will be the base-line case when we examine the interplay between melt dynamics and hydraulic control in section 3. When we derive general results below, however, we will allow n_1 and n_2 to be arbitrary positive numbers, but subject to the constraint $n_1 > n_2$.

2.2.1 The melt-controlled exchange flow regime

Consider a situation in which the fjord geometry, via frictional resistance or hydraulic control, does not limit the exchange flow and its associated heat transport towards the ice tongue. We assume that unmodified AW reaches the glacier ($T_C = T_A$), and the melt processes create a plume volume flow Q_P that sets the exchange flow: If T_A increases also the exchange flow increases at the rate given by Eq. (16). This regime, in which the strength of the exchange flow is controlled locally by the glacier basal melt, will be referred to as the melt-controlled regime; and a contrasting hydraulically-controlled exchange flow regime will be presented in the next section.

In the melt-controlled regime, where $Q = Q_P$, we can use the heat-conservation relation (9) together with Eqs. (15,16) to obtain

$$\frac{\Delta T}{T_G} = \frac{\gamma_1}{\gamma_2} \mathcal{T}^{n_1 - n_2}. \qquad (18)$$

This relationship, which is equal to M/Q, shows that ΔT as well as the ratio M/Q increase with $\mathcal{T}$, i.e. the melt water fraction in the plume increases with thermal forcing. Note that the condition $n_1 - n_2 = 1$ yields a linear relation between ΔT as well as M/Q and the thermal forcing.

By dividing Eq. (18) with $\mathcal{T}/T_G$, we obtain

$$\frac{\Delta T}{\mathcal{T}} = \frac{T_G \gamma_1}{\gamma_2} \mathcal{T}^{n_1 - n_2 - 1}. \qquad (19)$$

Since $\mathcal{T} = \mathcal{T}_A$ in the melt-controlled regime, the left-hand side in this expression equals $(T_A - T)/(T_A - T_f)$; which is less or equal to one since $T \geq T_f$. When $n_1 - n_2 = 1$, the right-hand side becomes independent of $\mathcal{T}$ and equals

$$\sigma \overset{\text{def}}{=} \frac{T_G \gamma_1}{\gamma_2}. \qquad (20)$$

This parameter is a non-dimensional measure of the temperature of the outflowing glacially-modified water (T): when $\sigma = 1$, $T = T_f$; and when $\sigma = 0$, $T = T_A$. (This interpretation of the Eq. (19) applies also when $n_1 - n_2 \neq 1$, but then $\Delta T/\mathcal{T}$ is no longer constant in the melt controlled regime.) As will be shown below, σ influences aspects of the hydraulically-controlled regime.

To summarise, the flow in the melt-controlled regime is specified by a knowledge of the AW properties T_A and S_A, which determines the thermal forcing $\mathcal{T} = \mathcal{T}_A$. In turn, this yields M, Q, and ΔT (Eqs. 15,16,18), and ΔS is obtained from Eq. (10).

We will now go on to examine how a hydraulically-controlled exchange flow affects the melt dynamics. For this purpose, it is useful to write Q_P as a function of the temperature difference. By using Eq. (18), we obtain

$$Q_P = \gamma_2 \left(\frac{\gamma_2 \Delta T}{\gamma_1 T_G} \right)^{\frac{n_2}{n_1 - n_2}}. \qquad (21)$$

This show the melt-controlled exchange flow increases with ΔT when $n_1 - n_2 > 1$.

2.3 Hydraulic control

Fjord and sill geometries may impose limits on the exchange flow, which in turn can potentially alter the basal melt dynamics. In particular, hydraulic control of a two-layer exchange flow over a sill sets an upper bound for the exchange flow (say Q_H), which is determined by the upstream height of the AW layer above the sill (h) and the layer density difference (Pratt and Whitehead, 2007). Exchange flow strengths below the critical value Q_H are unconstrained by the geometry, and are referred to as subcritical flows. Thus, it is conceivable that a sufficiently strong melt-driven exchange flow, or a high sill, can cause a transition from a subcritical flow to a critical, hydraulically-controlled flow (Pratt and Whitehead, 2007).

How the flow evolves as the melt-driven exchange flow (or the sill height) is gradually increased and approaches the hydraulically-controlled limit is complex and depends on fjord and sill geometry (Armi, 1986; Pratt and Whitehead, 2007;

Nycander et al., 2008). Observations from the Ryder and 79°N glaciers show that the inflow at the sills in front of the ice

tongues are hydraulically controlled, and that the thickness of the inflow layer is thin compared to the upper outflowing layer

210 (Jakobsson et al., 2020; Schaffer et al., 2020). This implies that the flow can be approximated by a one-layer hydraulic model

representing the inflowing AW layer. Two additional features allow for simplifications of the hydraulic model. First, the depth

of AW layer on the seaward side (upstream) of the sill is much larger than at the sill, which implies that the upstream AW inflow

velocity is negligible. Second, the inflow over the sill is confined in a channel that is small compared to the internal Rossby

radius, which allows the Earth's rotation to be neglected. In this situation, the maximum hydraulically-controlled volume flow

215 is given by (Pratt and Whitehead, 2007)

$$Q_H = Wh^{3/2} \left(\frac{2}{3}\right)^{3/2} \left(\frac{g\Delta\rho}{\rho_0}\right)^{1/2}, \tag{22}$$

where W is the cross-sectional width of the lower layer on the sill[1], h the height of the lower layer above the sill upstream

(Fig. 1), and g the gravitational acceleration. By using Eq. (12), Q_H can be written as

$$Q_H = k_H h^{3/2} (\Delta T/T_G)^{1/2}, \tag{23}$$

220 where we have introduced

$$k_H \stackrel{\text{def}}{=} W \left(\frac{2}{3}\right)^{3/2} [g(\beta S_A - \alpha T_G)]^{1/2}. \tag{24}$$

In the hydraulically-controlled regime, the exchange flow is given by Eq. (23), i.e. $Q = Q_H$. By using this in the heat

conservation relation Eq. (8), we obtain

$$M = k_H h^{3/2} (\Delta T/T_G)^{3/2}. \tag{25}$$

225 ## 2.4 Steady-state regimes: melt-controlled and hydraulically-controlled exchange flows

The results presented above suggest that there can exist two different flow regimes in a fjord with basal ice-tongue melting: One

where the exchange flow Q is determined locally by the basal-melt processes on the glacier, and one where it is hydraulically-

controlled. The two regimes have the following characteristics.

1. In the melt-controlled regime, the volume flow of the melt-water plume is smaller than the upper limit set by hydraulic

230 control, i.e. $Q_P < Q_H$. Accordingly, the sill does not constrict the exchange flow, which is specified by Eq. (16) (or 21).

The flow at the sill is subcritical (Pratt and Whitehead, 2007), and as result there is limited mixing between inflowing

and outflowing waters. Essentially, unmodified AW reaches the grounding line of the ice tongue (Fig. 1a), which implies

that the thermal forcing is given by $\mathcal{T} = \mathcal{T}_A$. Since the freezing temperature (T_f) is set by the grounding-line depth (and

S_A which to a good approximation can be taken as constant here), the thermal forcing at a specific glacier is externally

235 determined by the AW temperature (T_A).

---

[1]For simplicity, we assume a rectangular cross section, which implies that W does not depend on h. Note that the lower-layer width W may be smaller

than than the fjord width if inflow is confined in a deeper channel crossing the sill, which is the case for Ryder; see Fig. 1 in Jakobsson et al. (2020).

2. In the hydraulically-controlled regime, the plume volume flow exceeds the hydraulic limit, i.e. $Q_P > Q_H$. The exchange flow is now determined by Eq. (23), and the flow at the sill crest is critical, and it accelerates down the landward slope of the sill (Pratt and Whitehead, 2007). Here the flow becomes supercritical, and inflowing AW mixes with colder outflowing water (Price and O'Neil Baringer, 1994; Pratt and Whitehead, 2007; Jakobsson et al., 2020; Schaffer et al., 2020). This lowers the temperature of the water reaching the grounding line (Fig. 1b), i.e. $\mathcal{T} < \mathcal{T}_A$. Importantly, this implies that the thermal forcing is no longer directly set by $\mathcal{T}_A$: $\mathcal{T}_A$ is the external forcing, but the local thermal forcing $\mathcal{T}$ is determined by dynamics in the fjord. The relationship between $\mathcal{T}$ and $\mathcal{T}_A$ can be expressed as

$$\mathcal{T} = R \cdot \mathcal{T}_A, \tag{26}$$

where $R = R(\mathcal{T}_A, h)$ is a reduction factor which arises when the exchange flow is hydraulically controlled. Note that $R \leq 1$ in the hydraulic regime; in the melt-controlled regime $R = 1$.
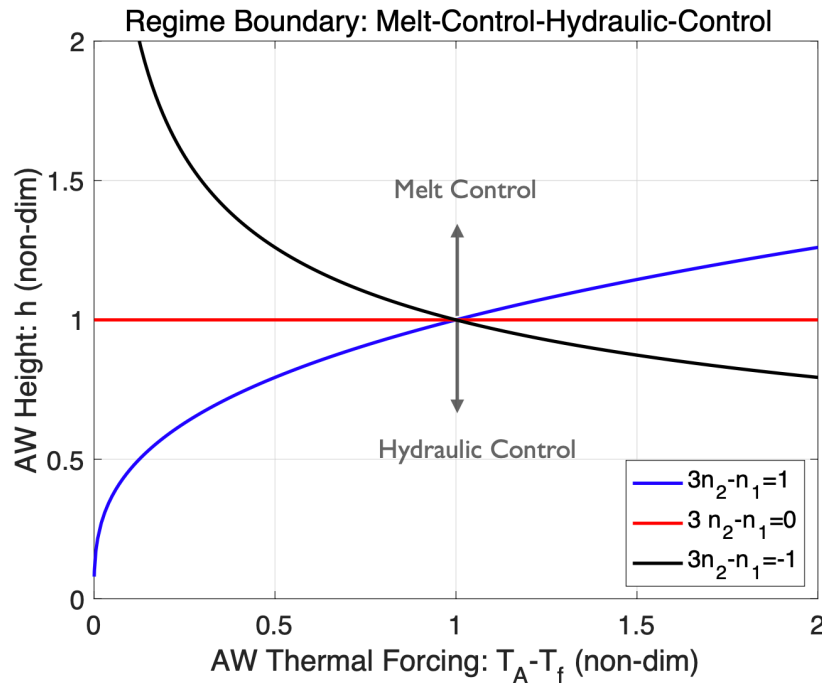

Figure 4. Regime boundaries between melt-controlled and hydraulically-controlled flows in the $\mathcal{T}_A-h$ plane (Eq. 27). The AW variables are non-dimensional. Hydraulically-controlled (melt-controlled) flows are found below (above) the lines, showing that the hydraulic regime is approached as h is decreased. When $3n_2 - n_1$ is positive (negative), the transition height h_L increases (decreases) with $\mathcal{T}_A$; and in the limiting case $3n_2 - n_1 = 0$, h_L is independent of $\mathcal{T}_A = T_A - T_f$.

At the transition between the two flow regimes $\mathcal{T} = \mathcal{T}_A$ and $Q_P = Q_H$, which implies that the transports given by Eqs. (21) and (23) are equal. By using this and Eq. (18), which applies at the transition, we obtain after some rearrangements

$$\frac{\gamma_1^{1/3} k_H^{2/3} h}{\gamma_2 \mathcal{T}^{\frac{3n_2 - n_1}{3}}} = 1. \tag{27}$$

This represents the condition $Q_P/Q_H = 1$, and gives the relationship between $\mathcal{T}$ and h at the regime transition. The height of

250 the AW above the sill at the transition (say h_L) as a function of $\mathcal{T}_A$ is given by

$$h_L = k_H^{-2/3} \gamma_1^{-1/3} \gamma_2 \mathcal{T}_A^{\frac{3n_2 - n_1}{3}}. \tag{28}$$

When $h > h_L$, the flow is in the melt-controlled regime, and when $h < h_L$, the exchange flow becomes hydraulically controlled. Alternatively, Eq. (27) gives the thermal forcing at the regime transition as a function of h

$$\mathcal{T}_L = \left(\frac{k_H^2 h^3 \gamma_1}{\gamma_2^3} \right)^{\frac{1}{3n_2 - n_1}}. \tag{29}$$

255 Using this and Eq. (18), the temperature difference at the regime transition can be written as

$$\frac{\Delta T_L}{T_G} = \frac{\gamma_1 \mathcal{T}_L^{n_1 - n_2}}{\gamma_2}. \tag{30}$$

If $n_1 - n_2 = 1$, then $\Delta T_L = \sigma \mathcal{T}_L$; see Eq. (20).

Lowering the AW height always brings the flow towards the hydraulic regime. If h is fixed also $\mathcal{T}_L$ is fixed, which implies that changes of the AW temperature can cause a transition between the melt-controlled and the hydraulically-controlled regimes.

260 As illustrated in Fig. 4, the nature of the transition depends on the value of the exponent $3n_2 - n_1$ in Eq. (27). If $3n_2 - n_1 > 0$ increasing $\mathcal{T}_A$ will bring the flow towards the hydraulically-controlled regime. On the other hand if $3n_2 - n_1 < 0$, decreasing $\mathcal{T}_A$ will brings the flow towards the hydraulically-controlled regime. This behaviour follows from the fact that $Q_P \propto \Delta T^{\frac{n_2}{n_1 - n_2}}$ and $Q_H \propto \Delta T^{1/2}$. In the case $3n_2 - n_1 = 0$, the regime transition height h_L is independent of $\mathcal{T}_A$. This is because Q_P and Q_H then has the same dependence on ΔT.

265 Figure 5 illustrates the relation between exchange flow and temperature difference (Eqs. 21,23) for the case $n_1 = 2$ and $n_2 = 1$, which implies that $Q_P \propto \Delta T$. Here, the flow is in the melt-controlled regime if $\Delta T < \Delta T_L$, or from Eq. (18) equivalently if $\mathcal{T}_A < \mathcal{T}_L$. By increasing ΔT, the flow increases and is shifted towards and into hydraulic control.

In the case where $3n_2 - n_1 < 0$, hydraulic control – for a fixed h – occurs for weak thermal forcing and exchange flow. In a real fjord, additional exchange flows driven by winds and tides may be larger than a model predicted weak hydraulic flow

270 (Jackson and Straneo, 2016). This can prevent establishment of hydraulic control and in effect yield an exchange flow in the melt-controlled regime. We will briefly discuss this case in section 3.2.5 .

It is possible that transitions between melt- and hydraulically-controlled regimes can also be caused by seasonal variations in subglacial discharge, even if the AW features remain unchanged. The reason is that the basal melt M increases with the subglacial discharge (Jenkins, 2011; Xu et al., 2013), which has pronounced seasonal cycle that tracks the surface melt on the

275 glaciers (e.g. Truffer and Motyka, 2016; Cai et al., 2017). Thus, it is possible that in some fjords the exchange circulation can
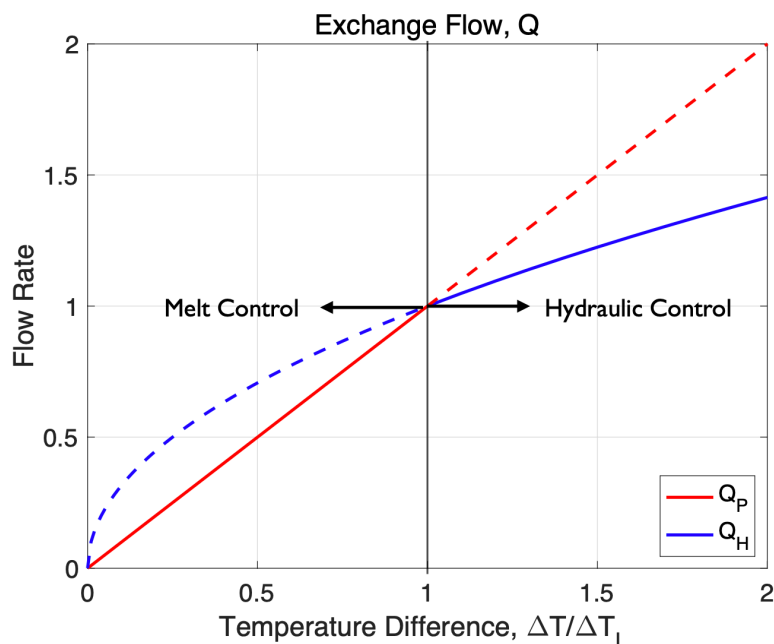
Figure 5. The hydraulically-controlled flow Q_H and the plume volume flow Q_P as functions of the layer temperature difference ΔT, for a fixed AW height (h). The case $n_1 = 2$ and $n_2 = 1$ is shown, and ΔT is normalised by ΔT_L (Eq. 30). The flow Q_H (blue lines) is proportional to $\Delta T^{1/2}$ (Eq. 23), and Q_P (red lines) is proportional to ΔT (Eq. 21). The solid lines show the actual exchange flow, which is set by the lower value of the two flows.

be stronger and hydraulically-controlled in summer when the subglacial discharge peaks, and weaker and melt-controlled in winter. The details of such seasonal regime transitions will depend, among other things, on how the ratio between exchange flow and melt (M/Q) depends on the subglacial discharge. However, we will not pursue this topic further.

3 The dynamics in the hydraulic regime

280 In the hydraulic regime, the volume flow of the melt plume is predicted to exceed the exchange flow at the sill (Fig. 5). This would cause an imbalance in production and export of glacially-modified waters in the fjord, preventing a steady state to be established. Therefore, changes of the flow are expected when hydraulic control is established.

To examine some of the new features emerging when the flow becomes hydraulically controlled, it is instructive to consider a thought experiment in which the sill height is suddenly increased and hydraulic control is established. Initially, the production

285 of glacially-modified water will be larger than the exchange flow across the sill. As a result, the layer of glacial water inside the sill will thicken and possibly extend below the sill crest (Fig. 1). This has two important consequences for the basal melt. First, the inflowing AW will entrain glacial water, causing the temperature of water reaching the grounding line to decrease.

Second, the melt-water plume will rise partly through ambient waters that are colder and lighter than the displaced AW. This reduces the buoyancy and speed of the plume, which now also will entrain colder water. Theses changes of the stratification in

290 the ice cavity act to reduce the basal melt. Thus, we expect that the temperature and salinity distributions inside the sill evolve such that a new steady state, compatible with the hydraulically-constrained exchange flow, is established.

The reasoning above and suggest that, in the hydraulic regime, the interface height of (pure or modified) AW is no longer the same on the seaward and landward side of the sill. Thus additional variables, such as a fjord interface height, may be needed to model flow- and melt-features in the hydraulic regime. However, we will not introduce additional model variable. Instead, we

295 consider two idealised scenarios for how the interplay between melt dynamics and hydraulic control can determine the steady state flow. In these scenarios, the features of the fjord stratification (i.e. interface height and layer difference of temperature and salinity) can be viewed as hidden model variables that influence the flow.

3.1 Scenario 1: Hydraulically constrained plume volume flow

3.1.1 Physical assumptions

300 Here, we assume that the steady-state flow and stratification inside the sill adjust such that:

1. The plume volume flow (Eq. 16) and the exchange flow (Eq. 23) are equal, which implies that $Q_P(\mathcal{T}) = Q_H(h, \Delta T)$.

2. The relationship between basal melt M and thermal forcing (Eq. 15) still applies and equals the formula for M in the hydraulically-controlled regime (Eq. 25). This gives a relationship of the form $\mathcal{T} = \mathcal{T}(h, \Delta T)$.

From these assumptions, we obtain the following expressions for the thermal forcing and temperature difference

305
$$\mathcal{T} = (k_H^2 h^3 \gamma_1 \gamma_2^{-3})^{\frac{1}{3n_2 - n_1}}, \tag{31}$$

$$\Delta T / T_G = \gamma_1 \gamma_2^{-1} (k_H^2 h^3 \gamma_1 \gamma_2^{-3})^{\frac{n_1 - n_2}{3n_2 - n_1}}. \tag{32}$$

Note that $\mathcal{T}$ and ΔT depend both on the features of the melt representation and the hydraulic constant k_H. In the reference case ($n_1 = 2$ and $n_2 = 1$) the exponents in the expressions above simplifies, and the hydraulic exchange flow (Eq. 23) becomes

310

$$Q_H = k_H^2 h^3 \gamma_1 \gamma_2^{-2}. \tag{33}$$

Notably, the flow is independent of the AW temperature T_A: The strength of the hydraulically-controlled flow is determined by h and the parameters γ_1, γ_2, and k_H, which control ΔT that is proportional to layer density difference.

3.1.2 Dynamical features

315 Figure 6 shows the dependence of the thermal forcing and the reduction factor on the AW forcing ($\mathcal{T}_A$ and h). The flow is in the hydraulic regime when $\mathcal{T}_A > \mathcal{T}_L$ and $h < h_L$, and opposite applies in the melt-controlled regime. In the melt-controlled
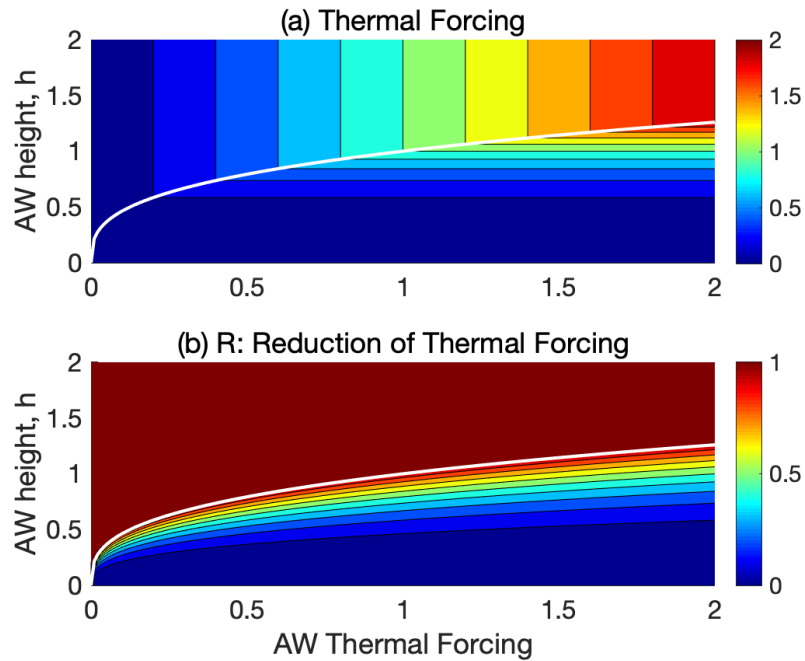
Figure 6. The dependence of the thermal ice-cavity forcing $\mathcal{T}$ (a) and the reduction factor R (b) on the AW thermal forcing ($\mathcal{T}_A$) and height (h) in scenario 1; see section 3.1. Here, $\mathcal{T} = T_C - T_f$ and $R = \mathcal{T}/\mathcal{T}_A$ (Eqs. 13, 26), implying that $R = 1$ in the melt-controlled regime. The non-dimensional variables are selected such that $\mathcal{T} = 1$ when $\mathcal{T}_A = 1$ and $h = 1$. The white line shows the boundary between the melt-controlled (above the line) and hydraulically-controlled regime (below the line). The case $n_1 = 2$ and $n_2 = 1$ is shown.

regime, $\mathcal{T}$ is equal to $\mathcal{T}_A$, and is independent of h. An increase in $\mathcal{T}_A$ or a decrease in h brings the flow towards the hydraulically-controlled regime. In this regime, the flow features become (in this scenario) independent of the AW temperature. As a result, the R factor decreases with increasing $\mathcal{T}_A$ at a fixed h. This provides a negative feedback on the basal melt. The flow features are sensitive to changes of h: when $n_1 = 2$ and $n_2 = 1$, one finds that $\mathcal{T} \propto h^3$ and $M \propto h^6$. Accordingly, the basal melt drops sharply with decreasing AW height.

In this hypothetical scenario, one should view $\mathcal{T}$ as an effective thermal forcing, which can have an implicit dependence on features such as the fjord stratification, rather than the actual thermal forcing near the grounding line (i.e., $T_C - T_f$). We expect that a a sudden increase of the inflowing AW temperature at the sill would initially cause warmer water to reach the grounding line and increase Q_P and M. However, adjustments of the temperature and stratification in the ice cavity are assumed to re-establish a state with the T_A independent melt rate determined by Eqs. (31) and (15). Since $\Delta T = T_A - T$ is constant, the outflow temperature T mirrors T_A.

3.2 Scenario 2: Unconstrained plume volume flow

3.2.1 Physical assumptions

330 We will now consider another hypothetical scenario in which the plume volume transport is determined by the thermal forcing via Eq. (16) and is not set directly by the hydraulic constrains. This implies that $Q_P > Q_H$, and additional physical processes need to be invoked to balance the production and export over the sill of glacially-modified water. Entrainment of some glacially-modified water into the inflowing AW, will help to achieve this balance: The entrained glacially-modified water is, in effect, re-circulating in the basin inside the sill. This can allow a steady state to develop even if Q_P exceeds Q_H. Specifically, in this

335 scenario, we assume that:

1. The excess volume flow in the plume is supplied by entrainment of glacially-modified water (Q_E) into the inflow of AW on the landward side of the sill:

$$Q_P = Q_E + Q_H. \tag{34}$$

By introducing the entrainment fraction (Price and O'Neil Baringer, 1994)

$$\Phi \stackrel{\text{def}}{=} \frac{Q_E}{Q_H + Q_E} = 1 - \frac{Q_H}{Q_P}, \tag{35}$$

we can relate the plume volume flow and the exchange flow as

$$Q_P = \frac{Q_H}{1 - \Phi}. \tag{36}$$

The parameter Φ ranges from 0 (no entrainment) to 1 (in the limit of strong entrainment).

2. The relationship between basal melt M and thermal forcing (Eq. 15) still applies and equals the formula for M in the
345 hydraulically-controlled regime (Eq. 25).

The second assumption yields the following relationship

$$\frac{\Delta T}{T_G} = \left(\frac{\gamma_1 \mathcal{T}^{n_1}}{k_H h^{3/2}} \right)^{2/3}. \tag{37}$$

By using this result in Eq. (23), we obtain

$$Q_H = \left(k_H^2 h^3 \gamma_1 \mathcal{T}^{n_1} \right)^{1/3}. \tag{38}$$

350 These formulas, which depend on features of the basal melt as well as h and k_H, specify the flow dependence on the thermal forcing in this hydraulic-regime scenario. However, $\mathcal{T}$ is a function of the AW forcing $\mathcal{T}_A$ and h that remains to be determined. This is obtained by considering how the grounding-line temperature is affected by entrainment of glacially-modified waters as outlined below.

The entrainment is controlled by local conditions on the landward side of the sill, where the denser inflowing AW accelerates
355 down the sill slope (Price and O'Neil Baringer, 1994; Pratt and Whitehead, 2007). However, we assume for simplicity that Q_E
adjust to satisfy Eq. (34). By using Eqs. (16,38), we can after some manipulations express the entrainment rate Φ as

$$\Phi = 1 - Z, \tag{39}$$

where

$$Z \overset{\text{def}}{=} \left(\frac{\gamma_1^{1/3} k_H^{2/3} h}{\gamma_2 \mathcal{T}^{\frac{3n_2 - n_1}{3}}} \right). \tag{40}$$

360 Here Φ is given by Eq. (39) when $Z \leq 1$, and when $Z > 1$ $\Phi = 0$. Note that $Z = 1$ yields the condition (Eq. 27) that defines
the flow-regime transition.

Next, we consider the relationship between the AW (S_A, T_A) and the water properties in the ice cavity (S_C, T_C), which are
affected by the entrainment: Conservation of heat in the cavity (see Fig. 1) yields

$$T_A Q_H + T Q_E = T_C (Q_H + Q_E). \tag{41}$$

365 By using the entrainment parameter Φ (Eq. (35), this yields the following expression for the temperature in the ice cavity

$$T_C = T_A - \Delta T \Phi. \tag{42}$$

Conservation of salt yields an analogous expression for S_C. Finally by using Eqs. (13,42), we obtain

$$\mathcal{T} = \mathcal{T}_A - \Delta T \Phi. \tag{43}$$

This relation and Eqs. (37,39) determine the functional relationship $\mathcal{T} = \mathcal{T}(\mathcal{T}_A, h)$ in this scenario. Note that since ΔT and Φ
370 are specified as functions of $\mathcal{T}$ and h, Eq. (43) also yields the function $\mathcal{T}_A(\mathcal{T}, h) = \mathcal{T} + \Delta T \Phi$, which is algebraically easier to
use when constructing graphical solutions. This is because the function $\mathcal{T}(\mathcal{T}_A, h)$ cannot, generally, be obtained on a closed
analytical form; see the appendix.

3.2.2 Dynamical features: general aspects

Figure 7 shows, for scenario 2, the dependence of the thermal forcing and the reduction factor on the AW forcing ($\mathcal{T}_A$ and
375 h). Again, the case $n_1 = 2$ and $n_2 = 1$ is illustrated, which is qualitatively representative for melt representations satisfying
$3n_2 > n_1$. Qualitatively, the behaviour is similar to that of scenario 1 (Fig. 6). A difference is that the thermal forcing now
increases with $\mathcal{T}_A$ in the hydraulic regime. However, the rate of increase is weaker than linear ($\frac{d\mathcal{T}}{d\mathcal{T}_A} < 1$).

For the hydraulically-controlled flow, entrainment of colder glacially-modified waters into the inflowing water lowers the ice
cavity temperature relative to T_A. This decreases the thermal forcing and thereby the melt rate: $\mathcal{T}$ decreases with decreasing
380 h and increases more slowly with $\mathcal{T}_A$ than in the melt-controlled regime. Figure 7b shows the reduction factor R (Eq. 26). By
definition $R = 1$ in the melt-controlled regime. In the hydraulic regime, $R < 1$, and the sensitivity of the thermal forcing to
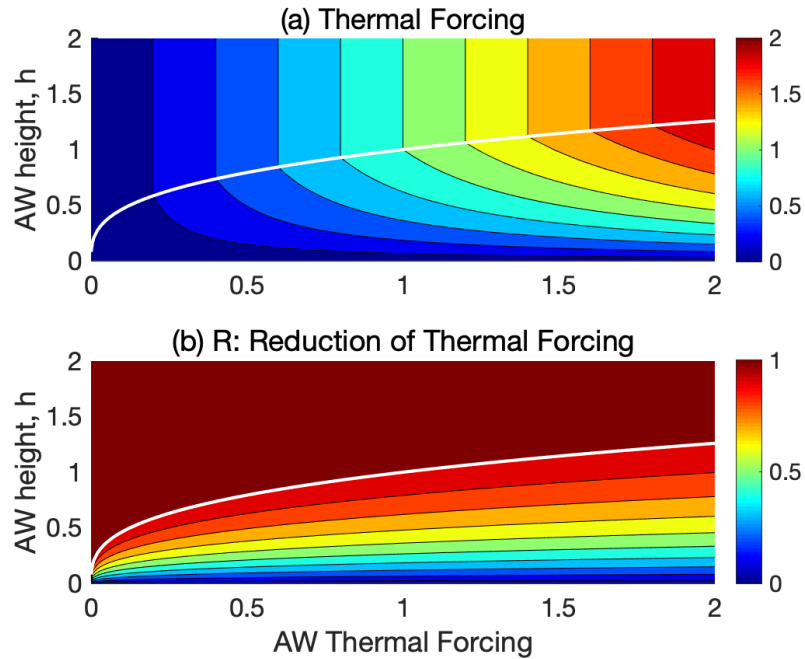
Figure 7. The dependence of the thermal ice-cavity forcing $\mathcal{T}$ (a) and the reduction factor R (b) on the AW thermal forcing ($\mathcal{T}_A$) and height (h) in scenario 2; see section 3.2. Here, $\mathcal{T} = T_C - T_f$ and $R = \mathcal{T}/\mathcal{T}_A$ (Eqs. 13, 26), implying that $R = 1$ in the melt-controlled regime. The white line shows the boundary between the melt-controlled (above the line) and hydraulically-controlled regime (below the line). The non-dimensional variables are defined as in Fig. 6. The case $n_1 = 2$ and $n_2 = 1$ is shown for $\sigma = 0.5$; see Eq. (20) and the text.

changes in $\mathcal{T}_A$ is reduced: the isolines of constant R becomes shallower with increasing $\mathcal{T}_A$. In the present scenario 2, the flow response depends also on the parameter σ, a non-dimensional measure of the outflow temperature T at the regime transition, which will be discussed below.

3.2.3 Dynamical features: dependence on AW height

Here, we examine the flow and melt response to changes in the AW height h for a fixed $\mathcal{T}_A$, i.e. moving vertically in Fig. 7. Specifically, we consider how the parameter σ affects the response. Recall that σ is a non-dimensional measure of the outflow temperature T in melt-controlled regime where $\Delta T/\mathcal{T}_A = \sigma$; see Eq. (20). We will consider the whole range of possible σ values ($0 \leq \sigma \leq 1$), but our observationally-based estimates indicate that σ is about 0.1 (Table 2).

Figure 8 illustrates how Q, entrainment fraction Φ, ΔT, $\mathcal{T}$ and M vary with the AW height h. (In the figures, we have normalised Q, $\mathcal{T}$ and M to be unity at the regime transition; but ΔT is normalised equal to σ.) If h is decreased, either by an increase in the sill height or by lowering the upper boundary of the AW, the flow is unchanged until $h = h_L$, the point at which the flow becomes hydraulically controlled. By further reducing h, Q, $\mathcal{T}$ and M decline but ΔT grows (implying decreasing

19

T). In the limiting case $\sigma = 1$, where ΔT is constant, Q is proportional to $h^{3/2}$; see Eq. (23). When $\sigma < 1$, Q falls less steeply

395   with h because the layer density difference (proportional to ΔT) increases with decreasing h.
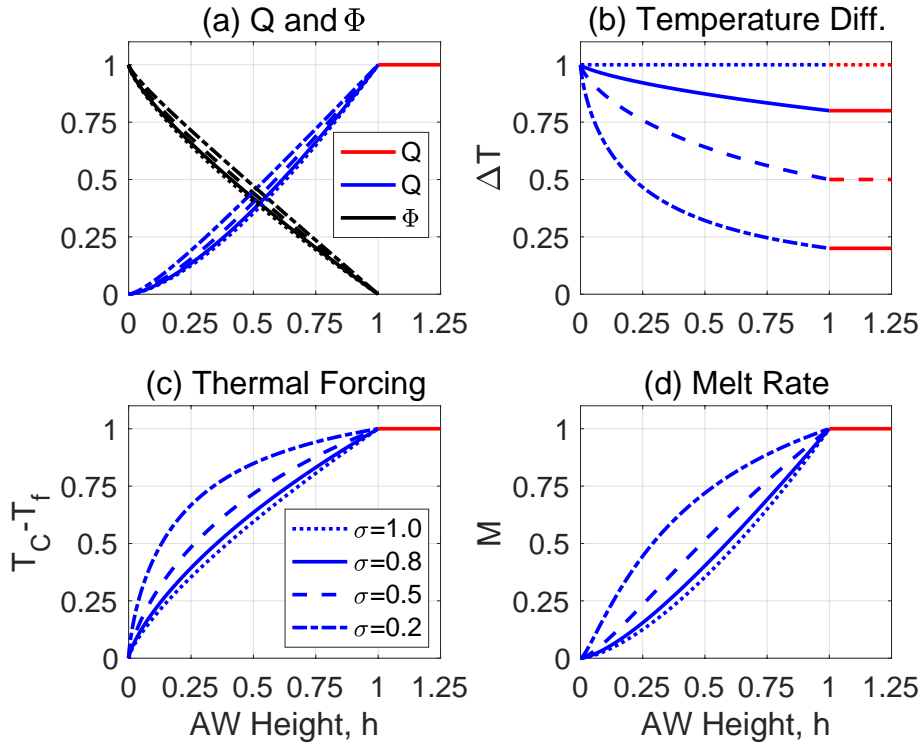

Figure 8. The flow dependence on the AW height h for a fixed value of $\mathcal{T}_A$. The case $n_1 = 2$ and $n_2 = 1$ is shown for different values of the non-dimensional parameter σ (Eq. 20); dotted, solid, dashed, and dash-dotted lines show results for $\sigma = 1.0$, $\sigma = 0.8$, $\sigma = 0.5$, and $\sigma = 0.2$, respectively. All variables are non-dimensional: the AW height h/h_L (Eq. 28) is smaller (greater) than one the hydraulic (melt-controlled) regime. (a) Exchange flow Q (blue and red lines) and entrainment fraction Φ (black lines), and (b) the temperature difference ΔT. (c) and (d) shows the thermal forcing ($\mathcal{T}/\mathcal{T}_A$) and melt rate. The melt rates are normalised to be unity in melt-controlled regime; dimensional melt rates are proportional to $\sigma^{3/2}$ (see the text).

In the hydraulic regime, outflowing glacially-modified water is entrained into inflowing AW, thereby reducing $\mathcal{T}$ (Fig. 8c). This effect is most pronounced for larger values of σ, which correspond to colder outflow temperatures of the glacially-modified water. In the limiting case $\sigma = 1$, $M \propto h^{\frac{3}{2}}$ because $\Delta T = \mathcal{T}_A$ is constant; see Eq. (25). The dependence of M on h in this limiting case describes the response for all values of σ when h/h_L becomes small. Here, $\Delta T/\mathcal{T}_A$ approaches its maximum

400   value of one. By using that $\Delta T \approx \mathcal{T}_A$ in Eq. (25), the melt rate becomes

$$M \approx k_H (h\mathcal{T}_A/T_G)^{3/2}. \tag{44}$$

Notably, the melt rate is independent of the features of the melt representation in this limit. From the melt rate formula (15), it follows that the thermal forcing is approximately given by

$$\mathcal{T} \approx \left(\frac{k_H h^{3/2}}{\gamma_1} \right)^{\frac{1}{n_1}} \left(\frac{\mathcal{T}_A}{T_G} \right)^{\frac{3}{2n_1}}. \tag{45}$$

405 Thus, the thermal forcing still depends on the melt parameterisation, but in such a way that the melt itself only depends on k_H, h and $\mathcal{T}_A$.

To summarise, in scenario 2 hydraulic control constrains the exchange flow and induces entrainment, which acts to lower the water temperature at the grounding line relative to T_A. Notably, when h/h_L becomes sufficiently small, the flow enters a regime where the exchange flow and the basal melt become independent of the physical processes near the ice–ocean interface 410 that govern the local melt rates. A partly analogous situation is an over-mixed estuary, where hydraulic control at a sill or a fjord mouth sets the exchange flow rate and vertical salinity difference independently of the nature of the mixing processes in the estuary (Stommel and Farmer, 1953; Timmermans, 1998).

3.2.4 Dynamical features: dependence on AW temperature

Next, we consider how the melt and flow features depend on the AW temperature when h is fixed. Figure 9 a and b show how 415 the exchange flow Q (normalised to be unity at the regime transition), temperature difference ΔT, the entrainment fraction Φ varies with the $\mathcal{T}_A$. In the melt-controlled regime, Q and ΔT depend linearly on $\mathcal{T}_A$ (when $n_1 = 2$ and $n_2 = 1$), and a larger σ is associated with a larger ΔT. If $\mathcal{T}_A$ is increased, the flow enters the hydraulically-controlled regime, where Q is proportional to $\Delta T^{1/2}$. This constrains the exchange flow, and increasing entrainment lowers the temperature at the grounding line. In response, the outflow temperature decreases, which causes ΔT to increase with $\mathcal{T}_A$ at rate that is slightly higher than 420 linear. In the limiting case $\sigma = 1$, $\Delta T = \mathcal{T}_A$ in both regimes and hence Q is proportional to $\mathcal{T}_A^{1/2}$ in the hydraulic regime. The entrainment rate depends only weakly on σ and increases relatively slowly with $\mathcal{T}_A$.

Figure 9 c and d show, the dependence of the thermal forcing and basal melt on $\mathcal{T}_A$, which both are normalised to be unity at the regime transition. In the hydraulic regime, $\mathcal{T}$ and M are for a given $\mathcal{T}_A$ lower than they would have been in a melt-controlled regime. Since $M \propto \Delta T Q$, the hydraulic-regime melt rate is proportional to $\mathcal{T}_A^{3/2}$ when $\sigma = 1$. Note that in Fig. 9, 425 the melt rates have been normalised to be unity at the regime transition for visual clarity. The actual melt rates are proportional to $\sigma^{3/2}$, implying that $\sigma = 1$ corresponds to the highest melt rate of a hydraulically-controlled exchange flow for a given $\mathcal{T}_A$.

3.2.5 Dynamical features: dependence on the melt dynamics

So far we have considered the case $3n_2 - n_1 > 0$, where increasing $\mathcal{T}_A$ brings the flow towards the hydraulic regime (Fig. 4). However, some qualitative different flow features emerge if $3n_2 - n_1 < 0$. This case seems less likely, but for completeness we 430 consider it briefly in the context of scenario 2. Figure 10 shows flow features for the cases $3n_2 - n_1 = 0$ and $3n_2 - n_1 = -1$. In the former case, the flow has the same dependence on ΔT in both regimes. As a result, the boundary between the flow regimes depends only on h. Further the R factor, the suppression of the thermal forcing due to hydraulic control, is independent of $\mathcal{T}_A$.
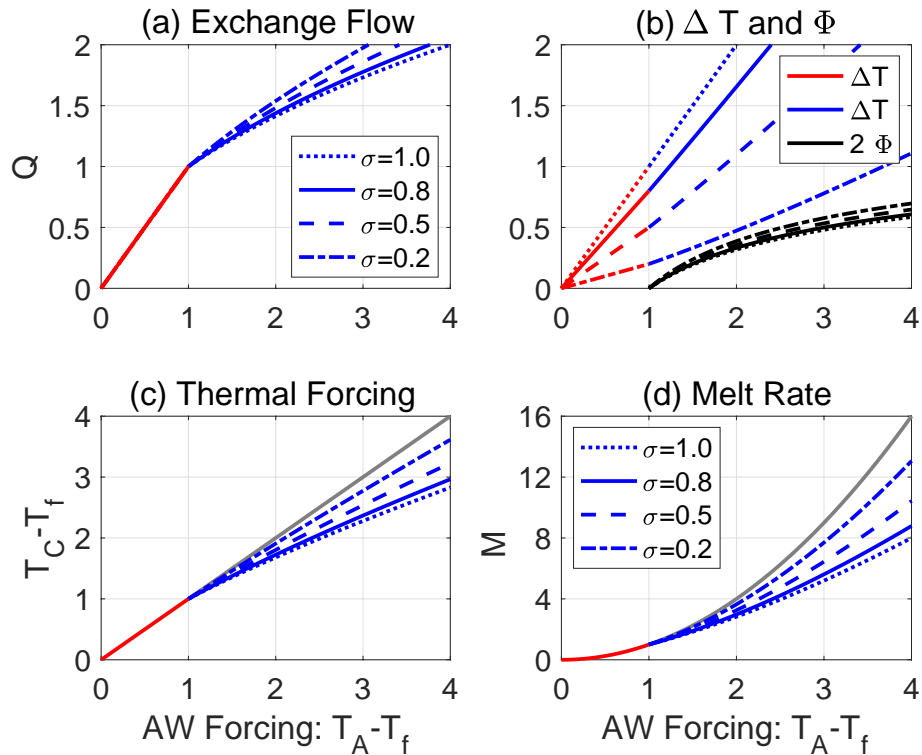
Figure 9. The flow dependence on the AW thermal forcing $\mathcal{T}_A$ for a fixed value of h. The case $n_1 = 2$ and $n_2 = 1$ is shown for different values of the non-dimensional parameter σ (Eq. 20); solid, dashed, and dash-dotted lines show results for $\sigma = 1.0$, $\sigma = 0.8$, $\sigma = 0.5$, and $\sigma = 0.2$, respectively. All variables are non-dimensional: the AW thermal forcing $\mathcal{T}_A/\mathcal{T}_L$ (Eq. 29) is greater (smaller) than one in the hydraulic (melt-controlled) regime. (a) Exchange flow Q and (b) temperature difference ΔT (red and blue lines), and entrainment fraction Φ (black lines); note that for clarity 2Φ is graphed. (c) Thermal forcing $\mathcal{T}$ and (d) and melt rate M; the grey lines show $\mathcal{T}$ and M in the melt-controlled regime extrapolated into the hydraulic regime. Note that M have been normalised to be unity at the regime transition; dimensional melt rates are proportional to $\sigma^{3/2}$ (see the text).

Also in the case $3n_2 - n_1 < 0$, the hydraulic control suppresses the thermal forcing and basal melt. However, here the R factor – for a fixed h – increases with increasing $\mathcal{T}_A$. Thus, as the AW temperature increases the hydraulic suppression of the melt decreases. Figure 10 (b) and (d) illustrate the limiting case $n_2 = 0$ where Q_P is a constant independent of the thermal forcing, but capture the qualitative features for the case $3n_2 - n_1 < 0$.

3.3 Applications to Ryder, 79°N, and Petermann glaciers

To examine some concrete aspects of the model, we will now apply it in a qualitative way to the ice tongues of Ryder, 79°N, and Petermann glaciers. We consider scenario 2, assuming $n_1 = 2$ and $n_2 = 1$, and try to crudely estimate model parameters charactering the melt–flow dynamics. We use observations of flow- and melt-rates (Q and M) and hydrography from the three
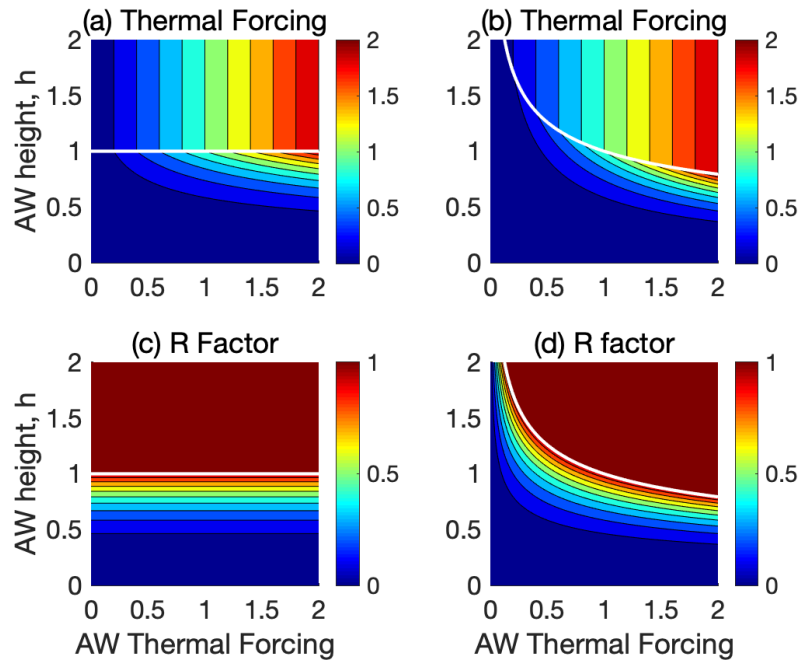
Figure 10. The dependence of the thermal ice-cavity forcing $\mathcal{T}$ (a,b) and the reduction factor R (c,d) on the AW thermal forcing ($\mathcal{T}_A$) and height (h) in scenario 2; see section 3.2. The non-dimensional variables are defined as in Fig. 6, $\sigma = 0.5$. The white line shows the boundary between the melt-controlled (above the line) and hydraulically-controlled regime (below the line). (a) and (c) show the case $n_1 = 1.5$ and $n_2 = 0.5$, for which $3n_2 - n_1 = 0$; and (b) and (d) show the case $n_1 = 1$ and $n_2 = 0$, for which $3n_2 - n_1 = -1$. Note that the case $3n_2 - n_1 < 0$ is less likely than the case $3n_2 - n_1 > 0$ shown in Fig. 7.

glaciers reported in the literature (Johnson et al., 2011; Wilson et al., 2017; Jakobsson et al., 2020; Schaffer et al., 2020). We recall that observations show that the sill exchange flows of Ryder and 79°N glaciers are hydraulically controlled, but that the exchange flow over the relatively deep and wide sill in Peterman Fjord is not. Note that there are uncertainties in the observations and in model assumptions, and the present exercise is primarily an illustration of how the model can be applied.

445   Guided by the model physics, we estimate model variables and parameters as follows: The hydrographic observations give T_C and T_A as the near-bottom temperatures inside and outside the fjord. The outflow model temperature T, which represents a flow-weighted mean over of an outflow distributed vertically over a range of temperaturs, is less straightforward to determine from hydrography. Here, we use the relation $M/Q = \Delta T/T_G = \Delta S/S_A$ [which follows from Eqs. (3,9)] to find values of T and S that roughly satisfy these conditions, and at the same time characterise outflowing water. This allows Φ to be determined

450   from Eq. (42).

Table 2. Observational features and estimated model parameters in scenario 2 (section 3.2) for Ryder, 79°N, and Petermann glaciers. See the text for details. In the model fit, it is assumed that $n_1 = 2$ and $n_2 = 1$. Note that the AW temperature T_A is the measured temperature on the seaward side of the sill closest to the ice tongue.

	Ryder Glacier	79°N Glacier	Petermann
A area (km^2)	300	1700	1000
M (m^3 s^{-1})	60	600	300
Q (10^3 m^3 s^{-1})	10	46	50
M/Q (%)	0.6	1.3	0.6
T_A, T_C (°C)	0.3, 0.2	1.8, 1.2	0.3, 0.3
$\mathcal{T}_A$, $\mathcal{T}$ (°C)	2.8, 2.7	4.2, 3.6	2.8, 2.8
$R = \mathcal{T}/\mathcal{T}_A$	0.96	0.86	1
ΔT (°C)	0.5	1.0	0.5
ΔS (g/kg)	0.2	0.5	0.2
Φ	0.3	0.6	0.0
γ_1 (m^3 s^{-1} °C^{-2})	8	46	40
γ_2 (m^3 s^{-1} °C^{-1})	$5 \cdot 10^3$	$3 \cdot 10^4$	$2 \cdot 10^4$
$k_H h^{3/2}$ (m^3 s^{-1})	$1.3 \cdot 10^5$	$4 \cdot 10^5$	
h_L (m), h/h_L	100, 0.7	220, 0.4	40, 3.4
σ	0.1	0.1	0.2

The model parameters γ_1, γ_2, and k_H are estimated as follows: From Eq. (15), we obtain $\gamma_1 \approx M/\mathcal{T}^2$. By using Eqs. (15,16,36), we obtain $\gamma_2 \approx Q/[\mathcal{T}(1-\Phi)]$. This provides the estimate

$$\sigma = \frac{T_G \gamma_1}{\gamma_2} \approx \frac{T_G M}{\mathcal{T} Q}(1-\Phi). \tag{46}$$

By using Eqs. (23,25), we obtain $k_H h^{3/2} \approx Q^{3/2}/M^{1/2}$; and an estimate of h then gives k_H. Note that k_H can also be
455 determined from a knowledge of the cross-sectional sill width W.

The estimates of Q from Ryder and Petermann are more uncertain than the ones from 79°N reported by Schaffer et al. (2020), which are based on a one-year moored time series of velocity. The Ryder estimate of Q is based on a single instantaneous current measurement on the inner sill in Sherard Osborn Fjord (Jakobsson et al., 2020). Our Petermann estimate of Q is based on hydrography and geostrophic velocities presented by Johnson et al. (2011): using their Fig. 7, we estimate the outflow of
460 glacially modified water (in the depth rage from 150 to 250 m) to be $50 \cdot 10^3$ m^3 s^{-1} (with large error bars).

Table 2 summarises observational features and estimated model parameters. Notably, the estimates of σ, around 0.1–0.2, are similar for the three glaciers. This reflects that the cooling due to ice melt of the melt-water plume is small compared to the upper limit ($\sigma = 1$), in which the outflow temperature ($\mathcal{T}$) approaches the freezing point. For Ryder and 79°N glaciers, which have hydraulically-controlled exchange flows, the estimated h/h_L is 0.7 and 0.4, respectively. The lower value of
465 h/h_L at 79°N Glacier implies a higher sensitivity of the melt to changes of h/h_L; see Fig. 8. Further, the reduction factors

($R = \mathcal{T}/\mathcal{T}_A$), which are directly inferred from the hydrography, are only slightly below unity: R is 0.96 and 0.86 at Ryder and

79°N, respectively. If as assumed here $M \propto \mathcal{T}^2$, this implies that, relative the situation where AW reaches the grounding line,

the melt rates are reduced by about 10 and 30 % at Ryder and 79°N, respectively. Taken together, this suggests that hydraulic

control and associated entrainment reduce the basal melt on both ice tongues, but that currently this effect is more pronounced

470   at 79°N Glacier.
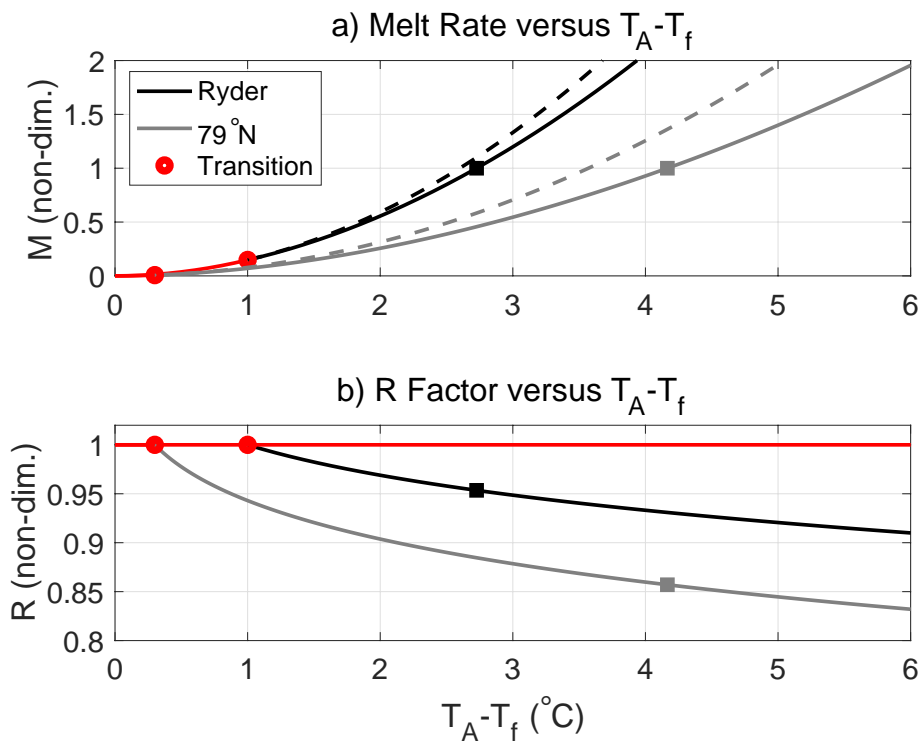
Figure 11. Model-based estimates of non-dimensional melt rate M (a) and R factor (b), for observed values of h, as a function the AW
thermal forcing $\mathcal{T}_A$ for Ryder (black lines) and 79° (grey lines) glaciers. Red lines shows the melt-controlled regime, and dashed lines in
(a) shows M if AW would reach the grounding line ($\mathcal{T} = \mathcal{T}_A$). The estimate is based on the model scenario 2 (see 3.2 and with $n_1 = 2$ and
$n_2 = 1$). The melt rates are normalised to be unity for the present observed values; see table 2 and section 3.3. The squares mark the observed
values of $\mathcal{T}_A$, and the red dots mark the model-predicted transition between the melt-controlled and the hydraulically-controlled regimes.

Figure 11 shows model-predicted melt rates M and R factors as a function of $\mathcal{T}_A$ for Ryder and 79°N glaciers when h is

kept at observed values. The figure also shows the melt rates that would occur if unmodified AW reached the grounding lines:

the melt rates in the hydraulically-controlled regime are lower and their dependence on $\mathcal{T}_A$ are weaker. The model results show

that a 1 °C increase of $\mathcal{T}_A$ from present values increases M with about 75 % and 50 % at Ryder and 79°N, respectively. The

475   basal melt is more sensitive to the same change in T_A at Ryder than at 79°N simply because $\mathcal{T}_A$ is larger at 79°N. For fractional

changes of $\mathcal{T}_A$, the response in basal melt is more similar: a 10 % increase of $\mathcal{T}_A$ yields an increase in M of about 15 % at

both glaciers. (Note that a 10 % increase of $\mathcal{T}_A$ corresponds to an increase of ~ 0.3 and ~ 0.4 °C of T_A at Ryder and 79°N, respectively.) In the absence of hydraulic control, where $M \propto \mathcal{T}_A^2$, the corresponding increase in M would be 20 %. Figure 12 shows the model-predicted dependence of Ryder basal melt on T_A and h. Currently, AW interface is about 30 m below the transition depth h_L at which hydraulic control ceases, i.e. a lifting of AW interface by about 30 m would bring the flow into the melt controlled regime.
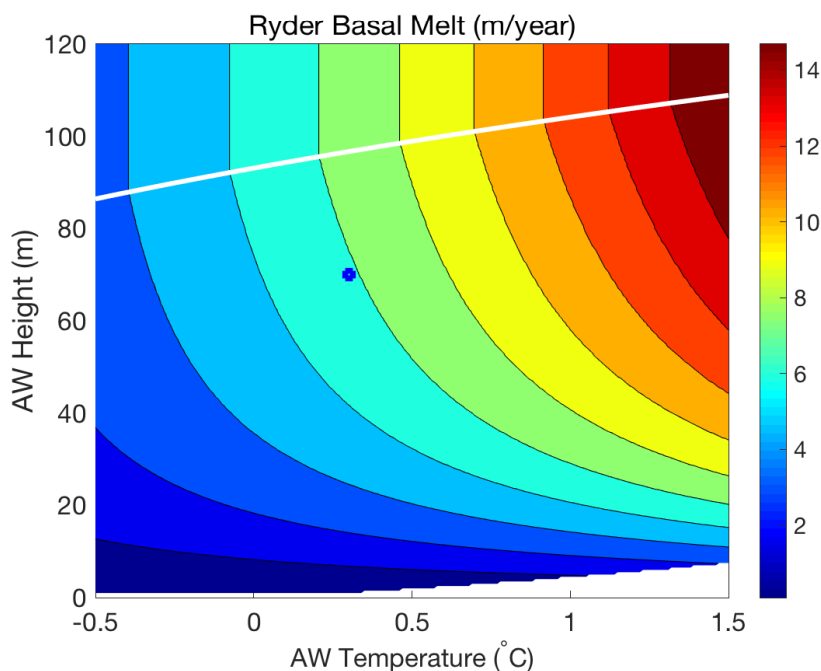
Figure 12. Estimated Ryder Glacier basal melt per unit area (M/A given in meters per year) as a function the AW temperature (T_A) and height (h) in model scenario 2; see section 3.2. Here, $n_1 = 2$ and $n_2 = 1$ and $M \propto \mathcal{T}^2$. The square indicates Ryders present state, and the white line shows the transition between the melt- and hydraulically-controlled regimes. In the white section in the lower right-hand side of the figure, the temperature leaving the glacier (T) is below the freezing point, and refreezing is expected to occur. See the text for details.

At Petermann Glacier, the exchange flow is not hydraulically controlled because the height of the AW above the sill is larger than the transition height h_L (Eq. 28). Note that h_L decreases with the cross-sectional width of the sill ($h_L \propto W^{-2/3}$). Ryder and Petermann have similar values of $\mathcal{T}_A$, and it is primarily the wide sill in Petermann Fjord that yields a small value of h_L (see Fig. 5 in Jakobsson et al., 2020).

4 Conclusions

To analyse the impact of hydraulic control on basal glacier melt, we have developed a two-layer fjord model that includes simple representations of melt and exchange-flow dynamics. Despite model idealisations, we believe that Figs. 6 and 7 qualitatively

illustrate how the interplay between near-ice melt processes and hydraulic control affects the relationship between basal melt

490 and AW features. Our results suggests that there are two flow regimes, with different relationships between basal melt and AW features. To begin with, a melt-controlled flow regime, in which the fjord geometry and sills do not restrict the exchange flow, and AW reaches the grounding line (Fig. 1). In this regime, the basal melt is rate limited by near-ice processes, rather than by the heat flux carried by the horizontal exchange flow in the fjord. Accordingly, the thermal forcing is set by the AW temperature and the basal-melt processes determine the strength of the exchange flow. In this regime, the dependence of the basal melt on

495 the AW height is weak and neglected here.

In a sill fjord, hydraulic control can set an upper bound on the exchange flow, which depends on the height of the AW above the sill crest and the density difference between the in- and out-flowing waters. If hydraulic control is established, the outflow of glacially-modified water created by the basal melt must be compatible with the hydraulically-determined exchange flow at the sill to ensure volume conservation. In a hydraulically-controlled flow regime, accordingly, the heat transport supplied by

500 the fjord circulation enters as a rate-limiting factor for the basal melt (Fig. 1). The flow can transit from a melt-controlled to a hydraulically-controlled regime if the AW height is decreased or the AW temperature is increased (Figs. 6,7). Such transitions can also occur when increasing subglacial discharge enhances the basal melt and the production of glacially-modified water.

In the hydraulic regime, decreasing AW height causes the exchange flow and its associated heat flux to decrease. As a result, the basal melt decreases. The hydraulic constraint also reduces the sensitivity of the basal melt to changes of the AW

505 temperature. We have examined this effect using a simple representation of the melt processes (Eqs. 15,16), and considered two idealised scenarios for how the flow adjusts to satisfy the hydraulic constraint; see sections 3.1 and 3.2. In these scenarios changes of the fjord stratification or entrainment of glacially-modified water into the inflowing AW are assumed to regulate the thermal forcing such that the hydraulic constraint is satisfied. In scenario 1 (Fig. 6), the thermal forcing is completely blind to the AW temperature, but sensitive to the AW height. Scenario 2 (Fig. 7) is less extreme, and here the thermal forcing has

510 a muted response to changes of the AW temperature, i.e. $\frac{d\mathcal{T}}{d\mathcal{T}_A} < 1$. These scenarios involve some fairly ad hoc assumptions, and further studies are needed to more accurately quantify the suppression of the thermal forcing in hydraulic flow regimes. Nevertheless, the qualitative features shown in Figs. 6 and 7 are expected to be robust.

The suppression of basal melt due to hydraulic control can be quantified by the reduction factor R (Eq. 26): the melt relative to the case when AW reaches the grounding line is proportional to R^{n_1}. At an ice tongue or tidewater glacier in a specific fjord,

515 R is a function of the AW features, i.e. $R = R(\mathcal{T}_A, h)$. This feature could be used to parametrise effects of hydraulic control in simulations of marine-glacier response to changes of AW forcing, which is crucial for the evolution of Greenlandic marine glaciers on decadal and centennial timescales (Straneo and Heimbach, 2013; Aschwanden et al., 2019; Wood et al., 2021).

We have considered a situation where the sill is seaward of the ice-tongue front, which is presently the case for Ryder and 79°N glaciers. However, if an ice tongue extends above the sill, the ice draft will contribute to the geometrical constraints that

520 determine the hydraulic exchange flow: the ice reduces the water-column depth over the sill. We will not explore this problem here. However, we note that in the early 1900s Ryder Ice Tongue was some 40 km longer that today, and covered the inner sill; its front reached roughly to the 82°12'N mark in Fig. 2c; see Jakobsson et al. (2020) and O'Regan et al. (2021) for additional

information. This should have strongly restricted the water exchange over the inner sill, resulting in very low basal melt on the inner part of the ice tongue.

525 Ryder Glacier has been relatively stable in recent decades (Hill et al., 2018). In contrast Petermann Glacier, located ∼200 km southwest of Ryder, have been retreating and lost 35 km of its ice tongue in 2010 and 2012 (Johannessen et al., 2013; Hill et al., 2018). Jakobsson et al. (2020) proposed that Ryder Glacier has been stable because of its more restrictive sill geometry, which partly protects the ice tongue from inflow of warmer subsurface AW (Fig. 2). The present study suggests that Ryder has a relatively high R value ($R \approx 0.9$), implying that despite the double sill geometry in Sherard Osborne Fjord, the modified AW

530 reaching the grounding line is currently weakly cooled as its flows through the fjord. However, the sensitivity of basal melt to thermal forcing depends on local conditions such as ice-tongue geometry, subglacial discharge and tidal currents. Notably, our simple model fit (Table 2) suggests that the thermal sensitivity of basal melt per unit area (γ_1/A) is 40 % higher for Petermann than for Ryder and 79°N glaciers, which have comparable sensitivities. Further, remote sensing analyses show that the basal melt per unit area (M/A) is about 50 % higher on Petermann than on Ryder (Wilson et al., 2017). Even if our model fit is quite

535 uncertain, this indicates that Ryder and 79°N glaciers, which are shielded by hydraulically-controlled sill flows, also have basal melt processes that are less sensitive to thermal forcing than Petermann.

We emphasise that the oceanic conditions at Ryder have only been observed a single time in the summer of 2019, and may not give a representative view of the melt–flow dynamic. As documented in the observations of Schaffer et al. (2020), variations of the AW height on monthly to annual timescales cause significant variations in exchange flow and basal melt. Thus,

540 in hydraulically-controlled fjords, long-term melt variations may be strongly controlled by the evolution of the AW height, a quantity that has received less attention than the AW temperature for the evolution of marine glaciers in Greenland (Straneo and Heimbach, 2013; Wood et al., 2021). Central Arctic Ocean observations document changes, on decadal timescales, of the AW height that are up to 100 m (Polyakov et al., 2004). If similar height changes would occur along the arctic coast of Greenland, significant changes in basal glacial melt would result: the present model (scenario 2) suggests that a lowering of the AW height

545 of ∼40 m would half the basal melt on Ryder Ice Tongue.

Appendix A

550 Here, we derive a few mathematical relationships that can be used to construct graphs for scenario 2. We assume that $n_1 - n_2 = 1$, which simplifies the algebra but is not strictly necessary.

When $\mathcal{T}_A$ is fixed h varies is convenient to put Eq. (43) on non-dimensional form using the variabels

$$\tilde{\mathcal{T}} \stackrel{\text{def}}{=} \frac{\mathcal{T}}{\mathcal{T}_A}, \qquad \tilde{h} \stackrel{\text{def}}{=} \frac{h}{h_L}, \tag{A1}$$

where h_L is defined in Eq. (28). Note that $\tilde{T} = R$; see Eq. (26). By using these non-dimensional variables and Eqs. (37,35),

555 we obtain

$$\tilde{T} = 1 - \sigma \frac{\tilde{T}^{\frac{2n_1}{3}}}{\tilde{h}} \left[1 - \tilde{h} \tilde{T}^{-(n_2 - n_1/3)} \right]. \tag{A2}$$

Here, the term in the square brackets on the right-hand side is Φ, and σ is defined by Eq. (20). From Eq. (A2), we can obtain $\tilde{h}$

as a function of $\tilde{T}$

$$\tilde{h} = \frac{\sigma \tilde{T}^{\frac{2n_1}{3}}}{1 - \tilde{T} + \sigma \tilde{T}}. \tag{A3}$$

560 It is generally not possible to find the inverse function $\tilde{T} = \tilde{T}(\tilde{h})$ on a closed analytical form, but Eq. (A3) allow us examine it

graphically by plotting $\mathcal{T}$ versus h. By using Eqs. (37,A3), we can after some manipulations find the dependence of ΔT and

Φ on $\tilde{T}$:

$$\frac{\Delta T}{\mathcal{T}_A} = 1 - \tilde{T} + \sigma \tilde{T}, \tag{A4}$$

565 $$\Phi = \frac{1 - \tilde{T}}{1 - \tilde{T} + \sigma \tilde{T}}. \tag{A5}$$

To examine the melt dynamics when h is fixed, it is useful to rewrite Eq. (43) as

$$\mathcal{T}_A = \mathcal{T} + \Delta T \Phi, \tag{A6}$$

where now the terms on the right-hand side are known functions of $\mathcal{T}$ and h specified by Eqs. (37,35). We put Eq. (A6) on

non-dimensional forms using the definitions of $\mathcal{T}_L$, ΔT_L, and h_L:

570 $$\frac{\mathcal{T}_A}{\mathcal{T}_L} = \frac{\mathcal{T}}{\mathcal{T}_L} + \sigma \left(\frac{\mathcal{T}}{\mathcal{T}_L} \right)^{\frac{2n_1}{3}} \left[1 - \left(\frac{\mathcal{T}_L}{\mathcal{T}} \right)^{\frac{3n_2 - n1}{3}} \right]. \tag{A7}$$

By using Eq. (A7), we obtain after some straightforward calculations

$$\left(\frac{d\mathcal{T}}{dT_A} \right)_{\mathcal{T} = \mathcal{T}_A} = \frac{1}{1 + \sigma(3n_2 - n_1)/3}, \tag{A8}$$

which applies at the regime transition in the hydraulically-controlled regime. In the melt-controlled regime, $\frac{d\mathcal{T}}{dT_A} = 1$. Thus,

the suppression of $\mathcal{T}$ relative to the AW thermal forcing ($\mathcal{T}_A$) is governed by the exponents n_1 and n_2, and σ. An inspection of

575 Eq. (35) shows that $(3n_2 - n_1)/3$ determines how fast the entrainment increases with $\mathcal{T}$.

Author contributions. JN lead the work on the paper. All authors contributed to the writing.

Competing interests. The authors have no competing interests.

References

Armi, L.: The hydraulics of two flowing layers with different densities, Journal of Fluid Mechanics, 163, 27–58, https://doi.org/10.1017/S0022112086002197, 1986.

Aschwanden, A., Fahnestock, M. A., Truffer, M., Brinkerhoff, D. J., Hock, R., Khroulev, C., Mottram, R., and Khan, S. A.: Contribution of the Greenland Ice Sheet to sea level over the next millennium, Science Advances, 5, https://doi.org/10.1126/sciadv.aav9396, 2019.

Cai, C., Rignot, E., Menemenlis, D., and Nakayama, Y.: Observations and modeling of ocean-induced melt beneath Petermann Glacier Ice Shelf in northwestern Greenland, Geophys. Res. Lett., 44, 8396–8403, https://doi.org/10.1002/2017GL073711, 2017.

Favier, L., Jourdain, N. C., Jenkins, A., Merino, N., Durand, G., Gagliardini, O., Gillet-Chaulet, F., and Mathiot, P.: Assessment of sub-shelf melting parameterisations using the ocean–ice-sheet coupled model NEMO(v3.6)–Elmer/Ice(v8.3), Geoscientific Model Development, 12, 2255–2283, https://doi.org/10.5194/gmd-12-2255-2019, 2019.

Gade, H.: Melting of ice in sea water: a primitive model with application to the Antarctic Shelf Ice and icebergs, J. Phys. Oceanogr., 9, 189–198, https://doi.org/10.1175/1520-0485(1979)009<0189:MOIISW>2.0.CO;2, 1979.

Gudmundsson, G. H.: Ice-shelf buttressing and the stability of marine ice sheets, The Cryosphere, 7, 647–655, https://doi.org/10.5194/tc-7-647-2013, 2013.

Hattermann, T., Smedsrud, L. H., Nøst, O. A., Lilly, J. M., and Galton-Fenzi, B.: Eddy-resolving simulations of the Fimbul Ice Shelf cavity circulation: Basal melting and exchange with open ocean, Ocean Modelling, 82, 28–44, 2014.

Hill, E. A., Carr, J. R., Stokes, C. R., and Gudmundsson, G. H.: Dynamic changes in outlet glaciers in northern Greenland from 1948 to 2015, The Cryosphere, 12, 3243–3263, https://doi.org/10.5194/tc-12-3243-2018, 2018.

Holland, D. M. and Jenkins, A.: Modeling Thermodynamic Ice–Ocean Interactions at the Base of an Ice Shelf, J. Phys. Oceanogr., 29, 1787–1800, https://doi.org/10.1175/1520-0485(1999)029<1787:MTIOIA>2.0.CO;2, 1999.

Holland, P. R., Jenkins, A., and Holland, D. M.: The Response of Ice Shelf Basal Melting to Variations in Ocean Temperature, Journal of Climate, 21, 2558–2572, https://doi.org/10.1175/2007JCLI1909.1, 2008.

Jackson, R. H. and Straneo, F.: Heat, Salt, and Freshwater Budgets for a Glacial Fjord in Greenland, Journal of Physical Oceanography, 46, 2735 – 2768, https://doi.org/10.1175/JPO-D-15-0134.1, 2016.

Jackson, R. H., Lentz, S. J., and Straneo, F.: The Dynamics of Shelf Forcing in Greenlandic Fjords, Journal of Physical Oceanography, 48, 2799–2827, https://doi.org/10.1175/JPO-D-18-0057.1, 2018.

Jakobsson, M., Mayer, L. A., Nilsson, J., Stranne, C., Calder, B., O'Regan, M., Farrell, J. W., Cronin, T. M., Brüchert, V., Chawarski, J., Eriksson, B., Fredriksson, J., Gemery, L., Glueder, A., Holmes, F. A., Jerram, K., Kirchner, N., Mix, A., Muchowski, J., Prakash, A., Reilly, B., Thornton, B., Ulfsbo, A., Weidner, E., Åkesson, H., Handl, T., Ståhl, E., Boze, L.-G., Reed, S., West, G., and Padman, J.: Ryder Glacier in northwest Greenland is shielded from warm Atlantic water by a bathymetric sill, Communications Earth & Environment, 1, https://doi.org/10.1038/s43247-020-00043-0, 2020.

Jenkins, A.: A one-dimensional model of ice shelf-ocean interaction, Journal of Geophysical Research: Oceans, 96, 20 671–20 677, https://doi.org/10.1029/91JC01842, 1991.

Jenkins, A.: Convection-Driven Melting near the Grounding Lines of Ice Shelves and Tidewater Glaciers, Journal of Physical Oceanography, 41, 2279 – 2294, https://doi.org/10.1175/JPO-D-11-03.1, 2011.

Johannessen, O. M., Babiker, M., and Miles, M. W.: Unprecedented retreat in a 50-year observational record for Petermann Glacier, North Greenland, Atmospheric and Oceanic Science Letters, 6, 259–265, https://doi.org/10.3878/j.issn.1674-2834.13.0021, 2013.

Johnson, H. L., Münchow, A., Falkner, K. K., and Melling, H.: Ocean circulation and properties in Petermann Fjord, Greenland, J. Geophys. Res. Oceans, 116, https://doi.org/10.1029/2010JC006519, 2011.

Khazendar, A., Fenty, I. G., and co authors: Interruption of two decades of Jakobshavn Isbrae acceleration and thinning as regional ocean cools, Nature Geoscience, 12, 277–283, 2019.

Lazeroms, W. M. J., Jenkins, A., Gudmundsson, G. H., and van de Wal, R. S. W.: Modelling present-day basal melt rates for Antarctic ice shelves using a parametrization of buoyant meltwater plumes, The Cryosphere, 12, 49–70, https://doi.org/10.5194/tc-12-49-2018, 2018.

Lazeroms, W. M. J., Jenkins, A., Rienstra, S. W., and van de Wal, R. S. W.: An Analytical Derivation of Ice-Shelf Basal Melt Based on the Dynamics of Meltwater Plumes, Journal of Physical Oceanography, 49, 917 – 939, https://doi.org/10.1175/JPO-D-18-0131.1, 2019.

Lewis, E. L. and Perkin, R. G.: Ice pumps and their rates, J. Geophys. Res., 91, 11 756–11 762, https://doi.org/10.1029/JC091iC10p11756, 1986.

Little, C. M., Gnanadesikan, A., and Hallberg, R.: Large-Scale Oceanographic Constraints on the Distribution of Melting and Freezing under Ice Shelves, J. Phys. Oceanogr., 38, 2242–2255, https://doi.org/10.1175/2008JPO3928.1, 2008.

Little, C. M., Gnanadesikan, A., and Oppenheimer, M.: How ice shelf morphology controls basal melting, J. Geophys. Res., 114, https://doi.org/10.1029/2008JC005197, 2009.

Morlighem, M., Williams, C. N., and co authors: BedMachine v3: Complete Bed Topography and Ocean Bathymetry Mapping of Greenland From Multibeam Echo Sounding Combined With Mass Conservation, Geophysical Research Letters, 44, 11,051–11,061, https://doi.org/10.1002/2017GL074954, 2017.

Mouginot, J., Rignot, E., Bjørk, A. A., van den Broeke, M., Millan, R., Morlighem, M., Noël, B., Scheuchl, B., and Wood, M.: Forty-six years of Greenland Ice Sheet mass balance from 1972 to 2018, Proceedings of the National Academy of Sciences, 116, 9239–9244, https://doi.org/10.1073/pnas.1904242116, 2019.

Nick, F., Vieli, A., Andersen, M., and co authors: Future sea-level rise from Greenland's main outlet glaciers in a warming climate, Nature, 497, 235–238, https://doi.org/10.1038/nature12068, 2013.

Nycander, J., Hogg, A. M., and Frankcombe, L. M.: Open boundary conditions for nonlinear channel flow, Ocean Modelling, 24, 108–121, https://doi.org/10.1016/j.ocemod.2008.06.003, 2008.

O'Regan, M., Cronin, T. M., Reilly, B., Alstrup, A. K. O., Gemery, L., Golub, A., Mayer, L. A., Morlighem, M., Moros, M., Munk, O. L., Nilsson, J., Pearce, C., Detlef, H., Stranne, C., Vermassen, F., West, G., and Jakobsson, M.: The Holocene dynamics of Ryder Glacier and ice tongue in north Greenland, The Cryosphere, 15, 4073–4097, https://doi.org/10.5194/tc-15-4073-2021, 2021.

Polyakov, I. V., Alekseev, G. V., Timokhov, L. A., Bhatt, U. S., Colony, R. L., Simmons, H. L., Walsh, D., Walsh, J. E., and Zakharov, V. F.: Variability of the Intermediate Atlantic Water of the Arctic Ocean over the Last 100 Years, Journal of Climate, 17, 4485 – 4497, https://doi.org/10.1175/JCLI-3224.1, 2004.

Pratt, L. J. and Whitehead, J. A.: Rotating Hydraulics: Nonlinear Topographic Effects in the Ocean and Atmosphere, Springer Verlag, first edn., 2007.

Price, J. F. and O'Neil Baringer, M.: Outflows and deep water production by marginal seas, Progress in Oceanography, 33, 161–200, https://doi.org/10.1016/0079-6611(94)90027-2, 1994.

Schaffer, J., T. Kanzow, W. J. v., L. von Albedyll, J. E. A., and Roberts, D. H.: Bathymetry constrains ocean heat supply to Greenland's largest glacier tongue, Nature Geoscience, 13, 227–231, https://doi.org/10.1038/s41561-019-0529-x, 2020.

Schoof, C.: Ice sheet grounding line dynamics: Steady states, stability, and hysteresis, J. Geophys. Res., 112, https://doi.org/10.1029/2006JF000664, f03S28, 2007.

655   Shroyer, E. L., Padman, L., Samelson, R. M., Münchow, A., and Stearns, L. A.: Seasonal control of Petermann Gletscher ice-shelf melt by the ocean's response to sea-ice cover in Nares Strait, Journal of Glaciology, 63, 324–330, https://doi.org/10.1017/jog.2016.140, 2017.

Stommel, H. and Farmer, H. G.: Control of salinity in an estuary by a transition, J. Mar. Res, 12, 13–20, 1953.

Straneo, F. and Cenedese, C.: The Dynamics of Greenland's Glacial Fjords and Their Role in Climate, Annual Review of Marine Science, 7, 89–112, https://doi.org/10.1146/annurev-marine-010213-135133, 2015.

660   Straneo, F. and Heimbach, P.: North Atlantic warming and the retreat of Greenland's outlet glaciers, Nature, 504, 36–43, https://doi.org/10.1038/nature12854, 2013.

Straneo, F., Sutherland, D., Holland, D., Gladish, C., Hamilton, G., Johnson, H., and Koppes, M.: Characteristics of ocean waters reaching Greenland's glaciers, Annals of Glaciology, 53, 202–210, https://doi.org/doi:10.3189/2012AoG60A059, 2012.

Stranne, C., Nilsson, J., Ulfsbo, A., O'Regan, M., Coxall, H. K., Meire, L., Muchowski, J., Mayer, L. A., Brüchert, V., Fredriksson, J.,

665   Thornton, B., Chawarski, J., West, G., Weidner, E., and Jakobsson, M.: The climate sensitivity of northern Greenland fjords is amplified through sea-ice damming, Communications Earth & Environment, 2, https://doi.org/10.1038/s43247-021-00140-8, 2021.

Timmermans, M.-L.: Hydraulic Control and Mixing in a Semi-Enclosed Reservoir, Tech. rep., Geophys. Fluid Dyn. Summer Study Program Tech. Rep. WHOI-98-09, 1998.

Truffer, M. and Motyka, R. J.: Where glaciers meet water: Subaqueous melt and its relevance to glaciers in various settings, Reviews of

670   Geophysics, 54, 220–239, https://doi.org/10.1002/2015RG000494, 2016.

Wilson, N., Straneo, F., and Heimbach, P.: Satellite-derived submarine melt rates and mass balance (2011–2015) for Greenland's largest remaining ice tongues, The Cryosphere, 11, 2773–2782, https://doi.org/10.5194/tc-11-2773-2017, 2017.

Wood, M., Rignot, E., Fenty, I., An, L., Bjørk, A., van den Broeke, M., Cai, C., Kane, E., Menemenlis, D., Millan, R., Morlighem, M., Mouginot, J., Noël, B., Scheuchl, B., Velicogna, I., Willis, J. K., and Zhang, H.: Ocean forcing drives glacier retreat in Greenland, Science

675   Advances, 7, https://doi.org/10.1126/sciadv.aba7282, 2021.

Xu, Y., Rignot, E., Fenty, I., Menemenlis, D., and Flexas, M. M.: Subaqueous melting of Store Glacier, west Greenland from three-dimensional, high-resolution numerical modeling and ocean observations, Geophysical Research Letters, 40, 4648–4653, https://doi.org/10.1002/grl.50825, 2013.

Zhao, K. X., Stewart, A. L., and McWilliams, J. C.: Sill-Influenced Exchange Flows in Ice Shelf Cavities, Journal of Physical Oceanography,

680   49, 163–191, https://doi.org/10.1175/JPO-D-18-0076.1, 2019.